Effect of hydrothermal carbonization pretreatment on the pyrolysis behavior of the digestate of agricultural waste: A view on kinetics and thermodynamics

Shule Wang, Yuming Wen, Ziyi Shi, Lukasz Niedzwiecki, Marcin Baranowski, Michal Czerep, Wangzhong Mu, Halina Pawlak Kruczek, Pär Göran Jönsson, Weihong Yang

Chemical Engineering Journal 431 (2022) 133881

Contents lists available at ScienceDirect

Chemical Engineering Journal

journal homepage: www.elsevier.com/locate/cej

Effect of hydrothermal carbonization pretreatment on the pyrolysis behavior of the digestate of agricultural waste: A view on kinetics and thermodynamics

Shule Wang [a], Yuming Wen [a,*], Ziyi Shi [a], Lukasz Niedzwiecki [b], Marcin Baranowski [b], Michał Czerep [b], Wangzhong Mu [a], Halina Pawlak Kruczek [b], Pär Göran Jönsson [a], Weihong Yang [a]

[a] KTH Royal Institute of Technology, Department of Materials Science and Engineering, Brinellvägen 23, 114 28 Stockholm, Sweden
[b] Wroclaw University of Science and Technology, Wybrzeże Stanisława Wyspiańskiego 27, 50–370 Wroclaw, Poland

ARTICLE INFO

Keywords:
Agricultural waste
Anaerobic digestion
Hydrothermal carbonization
Pyrolysis
Kinetics and thermodynamics
Kinetic prediction

ABSTRACT

Anaerobic digestion is the most promising disposal methods to treat organic waste. Also, a feasible management is necessary for the resulted digestate. Hydrothermal carbonization (HTC) combination with pyrolysis could be a proper solution to use for the treatment of digestate. In this study, the effect of an HTC on the pyrolysis of the digestate of agricultural waste (AWD) was investigated, focusing on the kinetic and thermodynamic aspects. Three model-free methods, including Friedman, KAS, and OFW methods, were used to evaluate the kinetic performance of the total and pseudo pyrolytic reactions of AWD and its hydrochar. Furthermore, kinetic predictions were made to provide more information for further studies. It was found that the HTC treatment decreased the activation energy ranges of the pyrolysis of AWD from 182.9–274.43 kJ/mol to 144.59–205.20 kJ/mol by using the Friedman method. For a more thorough understanding of the effect of HTC treatment on the pyrolysis of AWD, the pyrolysis reactions of AWD and its hydrochar were divided into two pseudoreactions using the Fraser-Suzuki deconvolution method. The mean activation energy of the deduced pseudo 2 pyrolytic reaction of hydrochar was 175.64 kJ/mol, which was 28.11 kJ/mol less than that of AWD. In addition, the $\Delta H^{\ddagger}$ values of the pseudo 2 reactions of AWD and its hydrochar were 197.97 and 169.68 kJ/mol, respectively. The results of kinetic isothermal predictions suggested that the peak temperature for the further research and application of the pyrolysis of AWD and its hydrochar should not be lower than 450 °C.

1. Introduction

Agricultural waste (AW) is the waste produced during agricultural activities, for instance, waste from farms and slaughterhouses [1]. Anaerobic digestion presents the potential to recover energy and materials from agricultural waste [2]. Anaerobic digestion has the advantage of producing methane from organic waste. The produced methane can be used as a biofuel or platform chemicals [3]. In general, anaerobic digestion has been widely applied to the management of agricultural waste. The digestate, solid residue from the anaerobic digestion process, is abundant in nutrients to be a candidate to use as a fertilizer [2,4]. The land application of digestate has been employed for a long time. However, due to the high nitrogen content contributed by the protein proportion in the AW, a relatively high nitrates content is formed in the digestate [5]. Using agricultural waste digestate (AWD) as fertilizer could result in saltilization, eutrophication, and organics pollution of the soil and underground water. EU has introduced the European Nitrates Directive (91/676/EEC), which limits the land application of the digestate [6]. Therefore, the digestate is required to be managed in a more sustainable way.

The abundant organic content in digestate makes it suitable to be used as a potential renewable fuel source. Previous researches have focused on producing char, liquid, and gas from digestate through pyrolysis [7–11]. The resulted char has been investigated as a soil amendment [12], activated carbon [13], carbon sink [14], or adsorbent for wastewater treatment [15]. The liquid product has been characterized for the application to replace fossil fuel [16] and for nutrient recovery [17]. The gas product was studied as gas fuel for electricity

* Corresponding author at: Brinellvägen 23, 114 28 Stockholm, Sweden.
E-mail address: yuming@kth.se (Y. Wen).

https://doi.org/10.1016/j.cej.2021.133881
Received 26 August 2021; Received in revised form 21 November 2021; Accepted 25 November 2021
Available online 1 December 2021

production.

Overall, there are some technical barriers related to the use of pyrolysis of digestate. One of the trickiest problems is the high moisture content of the digestate. Digestate contains approximately 70% moisture content after the mechanical dewatering process [18], because the water is trapped as bound water and capillary water in the matrix of digestate. The energy consumed for evaporation of the moisture content in digestate during the drying process limits the energy application of the digestate [9]. Nevertheless, the high moisture content also contributes to an increase in the cost of transportation and storage [19].

Hydrothermal carbonization (HTC), also named wet torrefaction, is a thermal chemical valorization process that can carbonize the feedstock [20]. Reported process temperatures vary significantly, ranging between 160 °C and 250 °C [21–24]. Also, the pressure is typically autogenic and is created during the process by evaporated water and gaseous products of the process (mainly CO_2). The pressure is high enough to keep most of the water as liquid at the temperatures achieved during the process. From a practical perspective, high pressure involves an increase in the thickness of the reactors' walls. Therefore, demonstration units typically target the lowest possible temperatures, allowing to obtain the desired effects on the feedstock at the lowest possible pressure. Thus, typically temperatures close to 200 °C are selected for operational pilot/demonstration scale units [25]. HTC has been widely applied to produce hydrochar from wet organic feedstocks [26–29]. The HTC can convert the hydrophilic groups on the surface of digestate into hydrophobic groups, which would enhance the dewaterability of the digestate [30]. With the use of an HTC process to pretreat the digestate, the moisture content of the hydrochar could reach 50% after a mechanical dewatering process [31]. A new approach of combining the HTC, mechanical dewatering, and pyrolysis for digestate management is proposed [32]. Stemann et al. have simulated the energy distribution on this new approach and found that it was feasible to dispose of digestate with respect to energy purposes [33].

There are some studies available that have focused on the effect of HTC on the pyrolysis of biomass and waste. Garlapalli et al. investigated the influence of HTC on the produced char from digested corn silage and cow manure [34]. Compared to pyrolysis of the digestate, the pyrolysis of the hydrochar from digestate can produce char with higher surface areas, higher carbon contents, and lower polycyclic aromatic hydrocarbon (PAH) contents [34]. Olszewski et al. found that using HTC as a pretreatment of pyrolysis of spent grains could yield chars with better physicochemical properties, including higher carbon contents and lower ash contents [35]. Mechanism studies are critical for designing the application of the HTC and pyrolysis on the treatment of biomass and waste. Another study conducted by Olszewski et al. reported the pyrolysis kinetics parameters of raw and HTC-treated spent grains [36]. Li et al. compared the kinetics and the intensity of the produced volatile of the pyrolysis of pinewood sawdust and its hydrochar using a thermogravimetric analyzer coupled with a Fourier transform infrared spectrometry (TG-FTIR) [37]. However, the kinetic and thermodynamic study of HTC pretreatment influence on the pyrolysis of digestate is remaining scarce, specifically for that of AWD. Thus, a comprehensive investigation of the pyrolytic kinetics and thermodynamics of AWD and its hydrochar from different aspects should be able to contribute to the understanding of the HTC pretreatment's effect on the pyrolysis of AWD. Moreover, kinetic predictions based on the resulted kinetic data can provide a solid reference for relevant future research and applications.

Model-free methods can be used to compute the kinetic parameters without making any assumptions on the reaction mechanism [38]. AWD and its hydrochar are both complex mixtures, which makes their thermal decomposition reactions to be sums of a series of different single reactions. Thus, using the model-free methods can avoid assuming the reaction mechanisms of the pyrolysis of AWD and its hydrochar. The model-free methods of Friedman, Kissinger-Akahira-Sunose (KAS), and Ozawa-Flynn-Wall (OFW) methods are used to calculate the kinetic parameters of the pyrolysis of AWD and its hydrochar in this study. Because these three model-free methods have been widely applied to analyzed the kinetic properties of the pyrolysis reactions [38–41]: their effectiveness has been examined and recognized. Moreover, the yielded kinetic data from this study can easily be compared to other studies using the same model-free methods.

In this study, for the first time, the effect of HTC pretreatment on AWD's pyrolysis behavior has been investigated using thermogravimetry (TG) experiments. The Fraser-Suzuki deconvolution method has been employed to identify and separate the pseudo single-step conversion curves from the master conversion curve. The pyrolytic kinetic and thermodynamic parameters of the total and pseudo reactions of the AWD and its hydrochar have been estimated. Model-free methods, including Friedman, KAS, and OFW methods, are applied to estimate the kinetic parameters. Thereafter, kinetic predictions are performed based on the obtained kinetic results.

2. Materials and methods

The diagram of the experiment and analysis process is shown in Fig. 1. Model-free methods were used in the kinetic analysis. The kinetics and thermodynamics of the pyrolysis of AWD and its hydrochar were estimated by focusing on two aspects: pseudo and total reactions. The analysis based on the pseudoreaction could make a better understanding of the effect of HTC on the pyrolysis kinetics and thermodynamics of AWD. On the other hand, the kinetic and thermodynamic analysis results of the total reaction of pyrolysis of AWD and hydrochar could be used for kinetic predictions. The details of the materials preparations, the used experimental and analytic methods are given below.

2.1. Raw materials

The original AW, mainly consist of cow dung, was digested anaerobically in an agricultural biogas plant located in the Silesia region, Poland to produce the AWD. The AWD sample was taken at the outlet of the reactor, prior to the mechanical dewatering stage. The AWD was stored in a fridge, at a temperature of 5 °C, before the HTC experiment. Furthermore, the carbohydrates in samples were determined by using SCAN-CM 71:09 methods at MoRe Research Örnsköldsvik AB, Sweden.

2.2. Hydrothermal carbonization treatment

Fig. 2 shows a diagram of the experimental setup. The autoclave vessel (Fig. 2 – 1), equipped with an external heating mantle that consisted of band heaters (Figs. 2 – 4), was filled with 3.8 L of wet AWD, which had a solids content of 10.1%.

The temperature of the heating mantle was controlled by a programmable logic controller (PLC) (Figs. 2 – 3). Additionally, the temperature was measured inside the reactor by using a K-type thermocouple inserted close to the center of the reactor (Fig. 2 – 2). A setpoint temperature of 190 °C was chosen, as the lower temperature of the typical HTC temperature range (180 °C and 260 °C) which have been recommended by various literature sources for digestates of agricultural origins [29,42] as well as other similar types of biomasses. The residence time in the reactor was 30 min. Reaching the setpoint temperature, the inside of the reactor triggered the time measurement. After 30 min of the process, the mantle was turned off and the setup was left for cooling. A colander (Figs. 2 – 6) and a clean cotton cloth (Figs. 2 – 5) were used for the subsequent separation of the effluent (Figs. 2 – 7) and hydrochar (Figs. 2 – 8). The cooled material was drained for approximately 20 min to let all the effluent be drained.

A Radwag MAX2A analyzer, with a scale resolution of 0.001 g and a maximum sample mass of 50 g, was used to determine the moisture content of the digestate and the dry solids content was obtained by the difference between the total value and the moisture content. All moisture content tests were performed at 105 °C. During an experiment, the

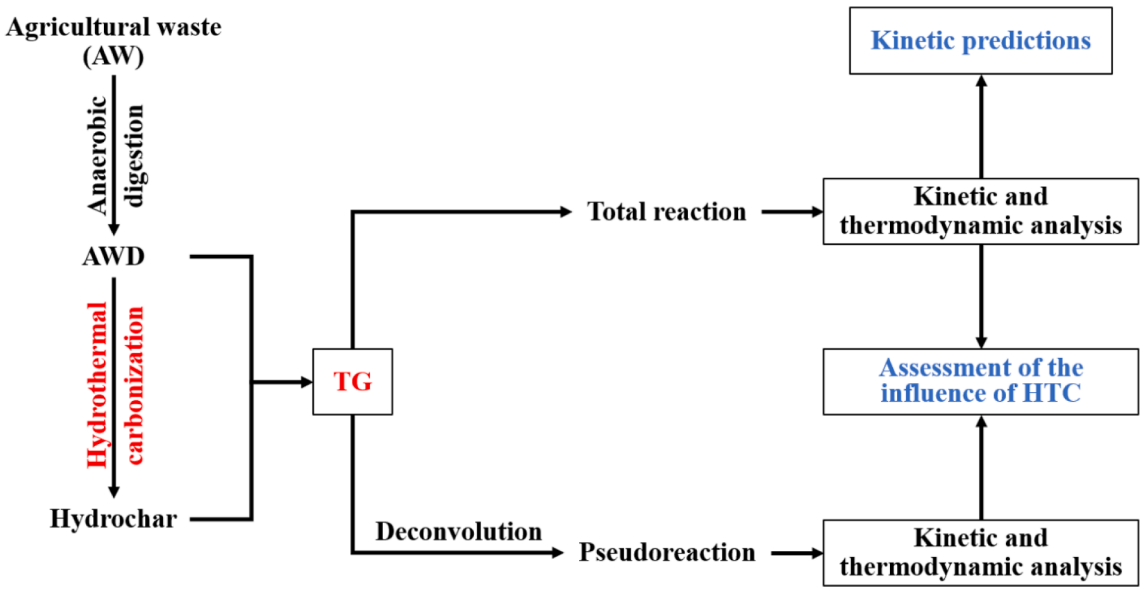

Fig. 1. The process of the raw materials and methods used in this study.

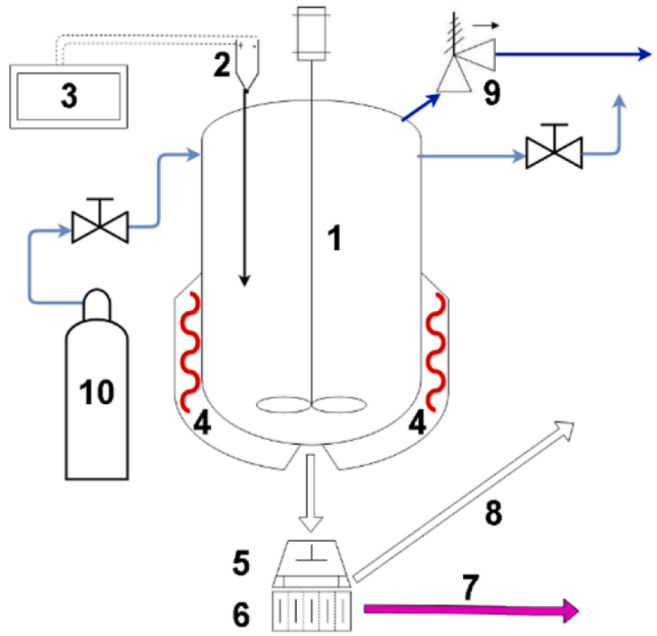

Fig. 2. Experimental setup, used for hydrothermal carbonization of the digestate (1 – autoclave; 2 – type K thermocouple; 3 – PLC controller; 4 – heating mantle, with band heaters; 5 – cotton cloth; 6 – colander; 7 – HTC effluent; 8 – hydrochar, after separation; 9 – pressure relief valve; 10 – nitrogen for purging).

sample's mass was considered to be in equilibrium when the first derivative of the mass (dm/dt) was equal to or smaller than 1 mg/min.

The dry AWD and hydrochar were characterized by the analytical company Eurofins AB to determine both ultimate and proximate components. The methods and corresponding uncertainties related to the measurement methods can be found in **Table S1**.

2.3. Sample preparation for pyrolysis

In order to minimize the random error of the sample composition and to achieve reliable results, a sample preparation is required before carrying out the TG experiments. The AWD and hydrochar were firstly dried in the drying oven at 110 °C for 24 h. Then, the dry samples were grinded and sieved to particles with a diameter less than 1 mm. Thereafter, the grinded samples were dried in the drying oven at 100 °C for another 24 h to remove the water that was absorbed during the grinding operation.

2.4. TG experiment

The TG experiments were performed using a Netzsch 449 F1 Jupiter simultaneous thermal analyzer (STA). The sample was introduced into an Al_2O_3 crucible placed in the heating chamber in a dry argon atmosphere. The flow rate of argon was chosen as 50 ml/min and the system was maintained under an atmospheric pressure during the whole TG experiment. During the TG experiments, the sample was ramped from room temperature to 120 °C and held at this temperature for 5 min to remove the moisture from the sample. Thereafter, the sample was heated to 900 °C using a constant heating rate of 10, 15, 20 °C/min. In order to minimize the system error, the TG instrument was calibrated by using a blank sample (empty crucible) and using the same experimental conditions.

The TG was coupled with a differential thermal analysis (DTA) system. In addition, the corresponding DTA results were also recorded.

2.5. Kinetic study

The AWD and hydrochar are complex mixtures consisting of organics, which include lignocellulose, lipids, proteins, and their derivates. The kinetic modeling was used for the investigation of the kinetic triplets of the samples. The thermal decompositions of the samples are first assumed to take place as one integrated reaction, shown in **Eq. (1)**:

$$Feedstock = Volatiles + Char$$

The kinetics of AWD and hydrochar thermal conversion were calculated based on Arrhenius law shown as **Eq. (2)**:

$$k(T) = Aexp\left(-\frac{E_a}{RT}\right)$$

where the A is the pre-exponential factor (min^{-1}), R is the universal gas constant equaling to 0.008314 kJ/mol, E_a is the activation energy (kJ/mol), and k(T) is the function of the reaction rate constant which depends on the temperature (T).

$$\alpha = \frac{m_0 - m_T}{m_0 - m_f}$$

where m_0, m_f, and m_T are the initial mass, final mass, and mass at a specific temperature T of reactant, respectively.

The reaction rate can be determined as described in the following equation:

$$\frac{d\alpha}{dt} = k(T)f(\alpha)$$

where t represents the reaction time, dα/dt represents the reaction rate, and f(α) is the function of the reaction model which is dependent on α.

When the feedstock is heated using a constant heating rate β (K/min), the following **Eq. (5)**, reaction model in an integral form g(α), can be derived by combining **Eq. (2)** and **Eq. (4)**.

$$g(\alpha) = \int_0^{\alpha} \frac{d\alpha}{f(\alpha)} = \frac{A}{\beta}\int_{T_0}^{T} exp\left(-\frac{E_a}{RT}\right)dT$$

2.5.1. Fraser-Suzuki deconvolution

In order to further investigate the effect of an HTC process on the kinetics and thermodynamics of pyrolysis of AWD, the Fraser-Suzuki deconvolution method is used to separate the pseudo-single-reactions from the total differential thermogravimetric (DTG) curves. The expression of the Fraser-Suzuki function is shown in **Eq. (6)**:

$$\frac{d\alpha}{dt} = hexp\left\{-ln(2)\left[\frac{ln\left(1+2a_s\frac{T-T_m}{w_{hf}}\right)}{a_s}\right]^2\right\}$$

where h is the height of a peak, a_s is its asymmetry, T_m is the temperature where the pseudo curve reaches its peak, and w_{hf} is the half-width of the pseudo curve [43]. The Fraser-Suzuki parameters of each pseudo curve were obtained by minimizing the residues between the total curve and the raw curve. In addition, the Fityk software (version 1.3.1) was used to conduct the optimization: by using the LogNormalA function, the software could yield the best fitting results based on the Fraser-Suzuki deconvolution method with the lowest errors.

2.5.2. Model-free methods

Model-free methods can be used to conduct the kinetic analysis without making any assumptions of the reaction mechanisms [44]. In this study, the three most-used model-free methods namely Friedman, KAS, and OFW methods were applied to analyze the kinetic parameters of the total and pseudo reactions of the pyrolysis of AWD and hydrochar. The expressions of the three model-free methods can be shown as follows [45]:

Friedman method

$$ln\left(\frac{d\alpha}{dt}\right) = ln[Af(\alpha)] - \frac{E_a}{RT}$$

KAS method

$$ln\left(\frac{\beta}{T^2}\right) = ln\left[\frac{AE_a}{Rg(\alpha)}\right] - \frac{E_a}{RT}$$

OFW method

$$log\beta = ln\left[\frac{AE_a}{Rg(\alpha)}\right] - 2.315 - 0.457\frac{E_a}{RT}$$

The corresponding kinetic parameters such as the activation energy E_a and the pre-exponential factor A were estimated following the recommendations of the International Confederation for Thermal Analysis and Calorimetry (ICTAC) [46] by using the NETZSCH Kinetics Neo software (ver. 2.5.0.1).

2.6. Activation parameters (thermodynamic analysis)

Transition status theory assumes a special type of chemical equilibrium (quasi-equilibrium) between reactants and activated transition state complexes. This theory makes it possible to investigate the thermodynamic parameters of the reaction from reactants to activated complexes. In this study, the transition status theory is introduced to investigate the influence of an HTC pretreatment on the behavior of a transformation from raw reactants to the activated transition state complexes. The activation parameters change in enthalpy ($\Delta H^{\ddagger}$), change in Gibbs free energy ($\Delta G^{\ddagger}$), change in entropy ($\Delta S^{\ddagger}$), during the conversion from reactants to the activated complexes, are derived using the following equations [47,48]:

$$\Delta H^{\ddagger} = E_a - RT$$

$$\Delta G^{\ddagger} = E_a + RT_m ln\left(\frac{K_B T_m}{hA}\right)$$

$$\Delta S^{\ddagger} = \frac{\Delta H^{\ddagger} - \Delta G^{\ddagger}}{T_m}$$

where T_m is the temperature of the peak of conversion rate (K), K_B is Boltzmann constant (1.381×10^{-23} J/K), and h is Plank constant (6.626×10^{-34} Js).

2.7. Kinetic prediction

By employing the kinetic parameters obtained from the kinetic analysis, isothermal kinetic prediction can be made using the following equation [49]:

$$t_{\alpha} = \frac{\int_0^T exp\left(\frac{-E}{RT}\right)dT}{\beta exp\left(\frac{-E}{RT_0}\right)}$$

where t_{α} and T_0 are the time and temperature when the reaction reaches the conversion degree of α, respectively.

3. Result and discussion

3.1. Feedstock ultimate and proximate analysis and Van Krevelen diagram

The results of sample characterization are shown in Table 1. AWD and hydrochar are the samples tested in this study. Characterizations of other samples from references are also listed as follows: cow manure digestate (CMD) and its hydrochar (CMDH), digestate containing 42 wt% cow manure, 20 wt% maize silage, 28 wt% grass silage, 9 wt% whole plant silage, and 1 wt% cereals (ECD) and its hydrochar (ECDH), municipal sewage sludge (MSS) and its hydrochar (MSSH) [42,50]. According to Table 1, the results of the proximate analysis of 4 groups of different digestates and their hydrochars from this study and other previous studies showed some similar trends: compared to the raw digestate, the hydrochar have higher fixed carbon and lower volatile matter contents. On the other hand, the trends of the ash content are different for different groups. These can be led by different types of ash in the digestates. The ash contents of AWD and its hydrochar are given in **Table S2**.

A Van Krevelen diagram can visualize the element ratios of O/C and H/C of samples [51]. Thus, it can be used to study the evolution of feedstocks and solid derivatives [52]. Based on the ultimate analysis results shown in Table 1, a Van Krevelen diagram was plotted as shown in Fig. 3. It can be concluded that the HTC treatment of digestate can lead to lower H/C and O/C ratios. Therefore, all four produced hydrochars had better potentials to be used as fuels compared to the raw

Table 1
Results of ultimate and proximate analyses of AWD and hydrochar.

	AWD	Hydrochar	CMD[a]	CMDH[a]	ECD[a]	ECDH[a]	MSS[b]	MSSH[b]
Proximate analysis								
Fixed carbon (% dw)	19.2	22.5	20.2	25.4	21.6	27.1	–	–
Volatile matter (% dw)	66.6	65.3	79.8	74.6	78.4	72.9	–	–
Calorific value of dry basis (MJ/kg)	20.89	22.49	17.0	17.6	16.4	15.7	17.55	16.74
Ash content (% dw)	14.2	12.2	15.7	17.2	28.7	28.9	33.14	46.65
Ultimate analysis (% dw)								
C	50.0	52.8	42.6	45.2	40.3	40.5	36.33	35.92
H	5.5	5.4	5.0	4.5	4.6	4.0	5.90	5.12
N	4.99	4.31	2.0	2.5	2.1	2.1	4.23	1.86
O*	23.88	24.66	34.3	30.2	24.0	24.1	12.81	7.96
S	0.70	0.39	0.4	0.4	0.3	0.4	–	–
Cl	0.73	0.24	–	–	–	–	–	–
Atomic H/C ratio	1.3106	1.2185	1.3984	1.1862	1.3600	1.1768	1.9349	1.6983
Atomic O/C ratio	0.3585	0.3506	0.6044	0.5015	0.4470	0.4467	0.2647	0.1663

dw: dewatering; *: Calculated by difference; [a]: data from reference [42]; [b]: data from reference [50].

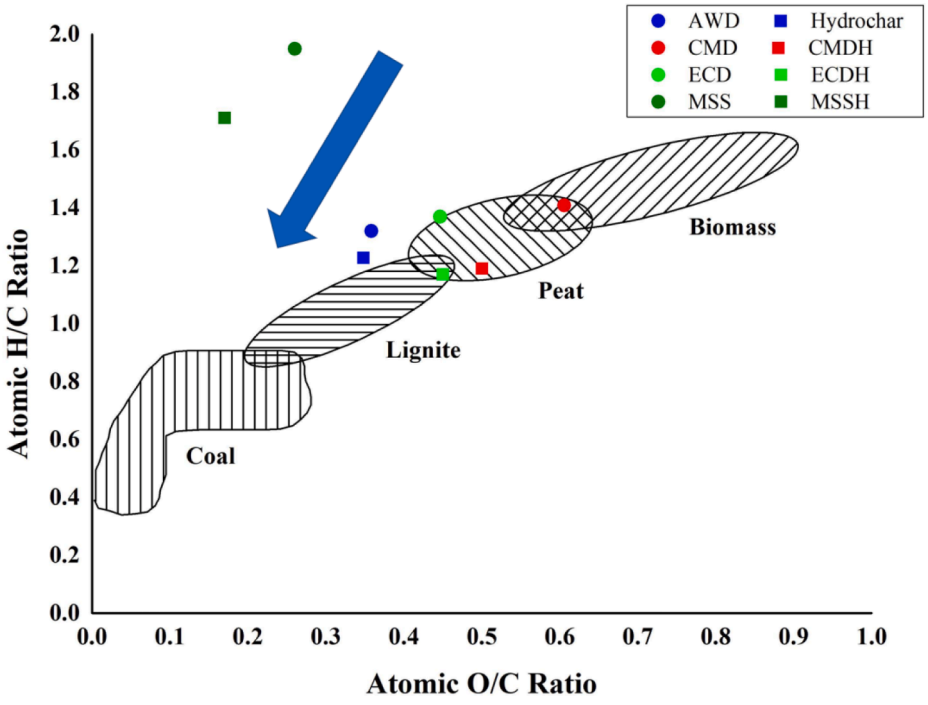

Fig. 3. Van Krevelen diagram of the AWD, hydrochar, and other raw and HTC-treated digestates from previous works [42,50]. (The blue arrow shows the trend from feedstock to its hydrochar).

digestates. The mechanism of HTC is complex and contains many chemical reactions that still need to be further investigated [53]. However, the lower ratios of H/C and O/C of hydrochars are probably due to the dehydration and decarboxylation reactions [20].

The contents of different carbohydrates of AWD and its hydrochar were also tested. The results are given in Table 2 and the method used is given in **Table S1**. By combing the results of the total contents of carbohydrates and the ash contents of AWD and its hydrochar, it can be deduced that the carbohydrates contents in the organic fractions of AWD and its hydrochar are 204.55 and 205.13 g/kg, respectively. Although the carbohydrates contained in the organic fraction of AWD were nearly the same after HTC treatment, the contents of different carbohydrates varies significantly as shown in Table 2. It can be seen that after the HTC treatment of AWD, the contents of arabinose, galactose, xylose, and mannose decreased from 16.3, 5.7, 54.6, and 3.0 g/kg to 2.6, 1.7, 21.9, and 1.9 g/kg, respectively. On the other hand, the glucose content of AWD increased from 95.9 to 152.0 g/kg by HTC treatment. The xylose is mainly contributed from hemicellulose [54]. Thus, more than half of hemicellulose in AWD decomposed during the HTC process while the

Table 2
Results of the analysis of the contents of different carbohydrates of AWD and its hydrochar.

	AWD (g/kg dw)	Hydrochar (g/kg dw)
Arabinose	16.3	2.6
Galactose	5.7	1.7
Glucose	95.9	152.0
Xylose	54.6	21.9
Mannose	3.0	1.9
Total carbohydrates	175.5	180.1
Cellulose*	53.8	83.9
Hemicellulose*	46.2	16.1

dw: dewatering; *: Calculate as % of carbohydrates in sample by using formulas **Eq. (S1)** and **Eq. (S2)** for hardwood.

The changes of the proximate and ultimate properties of AWD and hydrochar would lead to a different pyrolysis performance, which is required to be investigated.

cellulose in AWD remained its structure.

To have a better understanding of the changing of the contents of cellulose and hemicellulose of AWD by the HTC treatment, formulas to calculate the contents of cellulose and hemicellulose in hardwood were applied in this study and the results are also given in Table 2. There are different formulas to estimate the contents of cellulose and hemicellulose based on the contents of different carbohydrates. However, there is no appropriate formula for the relative calculation of digestates and their hydrochars. Because the relative content of cellulose and hemicellulose is changing during the anaerobic digestion process. Thus, it should be noticed that the calculated cellulose and hemicellulose contents might not be very accurate. It can be seen that the hemicellulose content of AWD was decreased from 46.2 to 16.1 % (total carbohydrates) after the HTC treatment. As a result, the cellulose content increased from 53.8 to 83.9 % (total carbohydrates). This is because, during the HTC treatment below 200 ℃, the hemicellulose tended to decompose while the cellulose remained in the matrix of hydrochar [55].

3.2. TG and DTG results

Fig. 4 gives the TG and DTG results of AWD and its hydrochar measured under different heating rates. The corresponding DTA results are given in **Fig. S1**. As shown in Table 3, approximately 35 and 21 mg of AWD and hydrochar were used in each experiment, respectively. It can be seen from the DTG curves that before the main mass loss happened, a small peak appeared in all cases. This is contributed by the evaporation of moisture and some light volatile matters [56]. When the temperature is higher than 600 °C, nearly no mass loss occurs. Therefore, temperature ranges of the main organic thermal decomposition were defined for each DTG result for the convenience and accuracy of further kinetic studies. The initial and final temperatures (T_i and T_f) were determined based on the lowest DTG points between the main mass loss peaks. The determined T_i, T_f, and peak temperatures (T_p) in this study are given in Table 3. The values of the T_i, T_f, and T_p of the pyrolysis of AWD and its hydrochar increase when the heating rate increases from 10 to 20 °C/min. This is mainly due to the limitations of the heat and mass transfer [57]. On the other hand, T_p of hydrochar is higher than that of AWD for each group of the same heating rate. The detail of this phenomenon will be discussed in **section 3.3** Kinetic analysis of the pseudoreaction.

3.3. Kinetic analysis of the total reactions

3.3.1. Kinetic plotting results of the total reactions

Fig. 5 gives the linear regression plotting results in the conversion rate ranges of 0.01 to 0.99 of the kinetic analysis of the total thermal

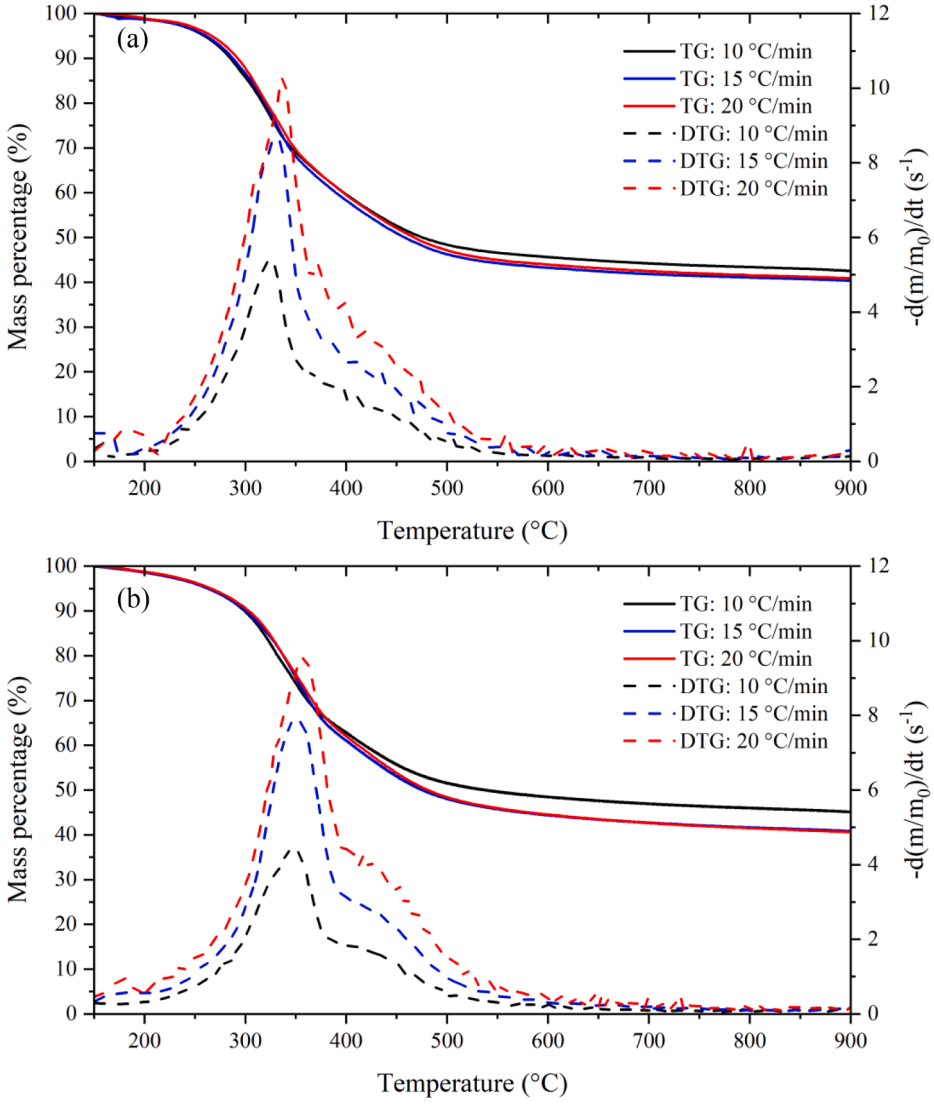

Fig. 4. TG and DTG curves of (a) AWD and (b) hydrochar, from 150 to 900 °C and for heating rates at 10, 15, and 20 °C/min.

Table 3
The mass used in each TG experiment and the selected temperature ranges for the kinetic analysis of AWD and hydrochar.

Heating rate	AWD				Hydrochar			
	Mass (mg)	T_i (°C)	T_p (°C)	T_f (°C)	Mass (mg)	T_i (°C)	T_p (°C)	T_f (°C)
10 °C/min	36.35	173	326	609	20.48	157	346	617
15 °C/min	34.69	183	330	613	19.93	164	350	624
20 °C/min	36.52	212	337	631	23.23	198	360	637

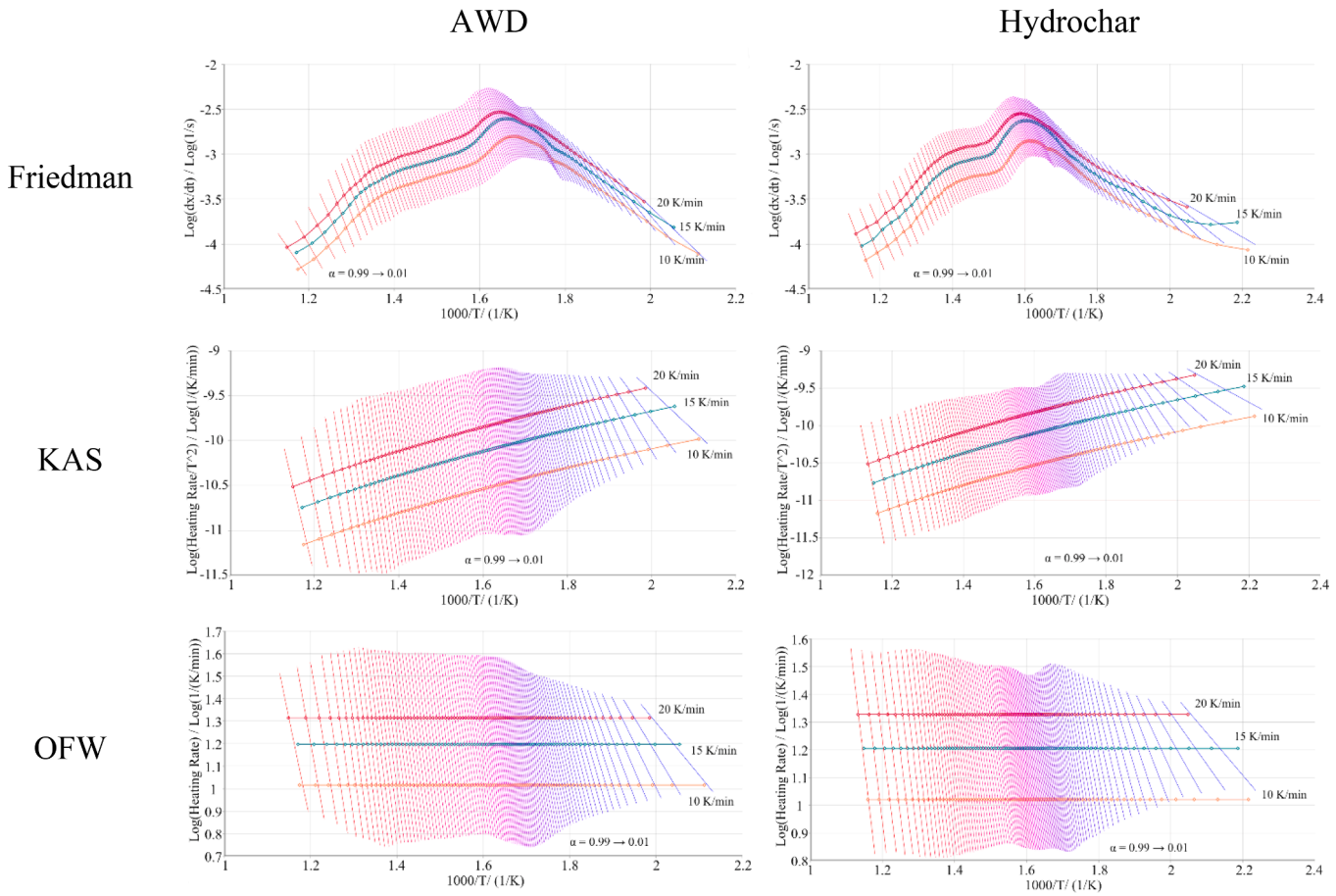

Fig. 5. Kinetic analysis of the total reactions of the pyrolysis of AWD and its hydrochar using the Friedman, KAS, and OFW methods.

decomposing reactions of AWD and its hydrochar by using different model-free methods. The temperature ranges of each reaction were determined and given in Table 3. The plotting results deduced by the KAS and OFW methods were similar compared to that of the Friedman method. This is because that the KAS and OFW methods were integral isoconversional methods [58] and the Friedman method is a differential isoconversional method [59]. The KAS and OFW results of AWD and its hydrochar contained dense parallel straight lines when the conversion rates are between 20% and 90%. This represents that the main reaction happened in this region. On the other hand, the plotting lines outside this range of conversion rate have obviously changing slopes and higher errors. These are caused by simultaneous reactions that take place as well as the presence of unstable radicals [60].

3.3.2. Activation energies of the total reactions

Based on the plotting results shown in Fig. 5, the corresponding activation energies and pre-exponential factors were estimated as shown in Fig. 6 and **Fig. S2**, respectively. The activation energy represents the difficulty of a reaction to take place [61]. When the conversion rate is between 20% and 90%, the yielded activation energies range from 182.91 to 274.43 kJ/mol (Friedman), 169.99–267.86 kJ/mol (KAS), and 170.16–268.05 kJ/mol (OFW) for the pyrolysis of AWD, and 144.59–205.20 kJ/mol (Friedman), 150.57–199.61 kJ/mol (KAS), and 150.83–199.87 kJ/mol (OFW) for that of hydrochar. Obviously, due to the same mechanisms of the applied methods, the activation energy of the pyrolysis of AWD or its hydrochar deduced by using the KAS and OFW methods were very similar.

The averagepyrolytic activation energies of AWD and OFW by the three methods are 242.13 kJ/mol and 167.97 kJ/mol, respectively. This result indicates that the pyrolysis of hydrochar requires a lower activation energy compared to that of AWD. The lower activation energy means that less energy is needed for the reaction to take place [62]. Thus, the HTC treatment can decrease the energy required for the pyrolysis of digestate, which favors the application of digestate in pyrolysis processes. The mechanisms of this phenomenon are discussed in section **3.4.3 Activation energies of the pseudoreactions**.

3.4. Kinetic analysis of the pseudoreactions

3.4.1. Fraser-Suzuki deconvolution results

The thermal decomposition reactions of AWD and its hydrochar are both complex reactions that include many different chemical reactions.

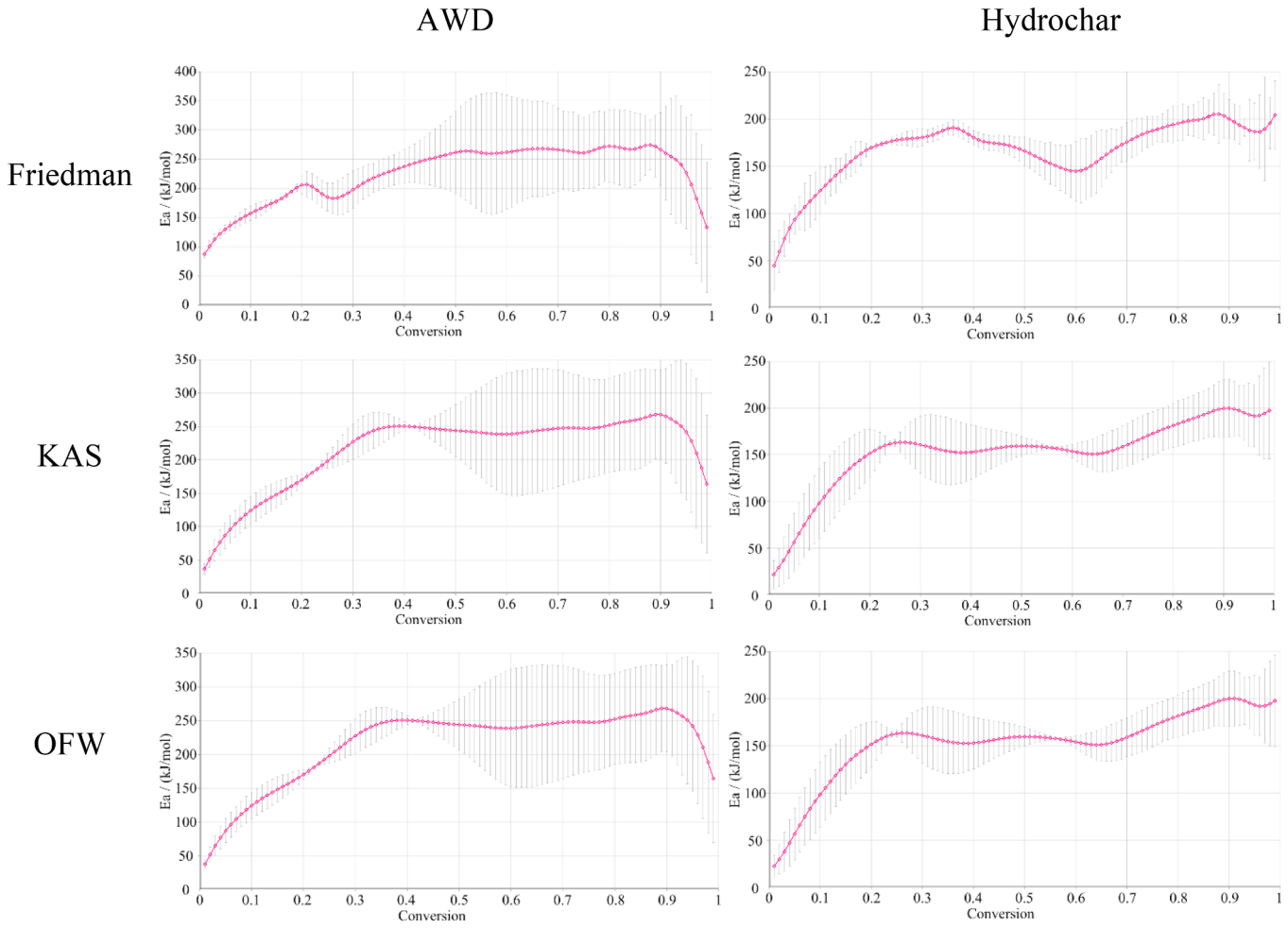

Fig. 6. Activation energies of the pyrolysis of AWD and its hydrochar deducing by using the Friedman, KAS, and OFW methods.

It is hard to investigate all the single reactions and their synergistic effects. However, introducing the mathematical deconvolution method to decompose the integrated reaction into several pseudo reactions can help to better understand the reaction mechanisms. The Fraser-Suzuki deconvolution is one of the most used mathematical deconvolution methods for TG research [63–65].

In this study, the total reactions of the pyrolysis of AWD and its hydrochar were divided into two pseudoreactions by using the Fraser-Suzuki deconvolution method. The reactions can be expressed as **Eq. (14)**: during the pyrolysis of the AWD or its hydrochar, the raw material was decomposed into volatile 1 (V1), volatile 2 (V2), and the remaining solid (char). It was assumed that the V1 and V2 were generated by pseudoreaction 1 and 2, respectively.

$$AWD/Hydrochar = V1 + V2 + Char$$

The deconvolution and the corresponding fitting results are shown in Fig. 7. It can be seen that all the deconvolution results showed an acceptable fitting level. The related deconvolution parameters are given in Table 4. The values of T_m of the pseudo 2 of AWD or its hydrochar increase with higher heating rates. These results are consistent with the DTG results.

The AWD used in this study was the digestate that was mainly produced from cow dung, which isa type of lignocellulose-riched materials: the main component of cow dung is lignin, cellulose, and hemicellulose [66]. During the anaerobic digestion process, the hemicellulose has a higher degradation rate than that of the cellulose and lignin, which then causes the cellulose and lignin to accumulate in the AWD [67]. Thus, the pyrolysis of AWD should be mainly contributed by the pyrolysis of its remaining cellulose and lignin. A previous work conducted by Stefanidis et al. compared the pyrolysis behaviors of cellulose, hemicellulose, and lignin under a heating rate of 10 °C/min: the results showed that the mainly decomposing temperature range of cellulose was between 280 and 360 °C with the highest decomposing rate at a temperature of 339 °C [68]. Moreover, they also found that the pyrolysis reaction of lignin happened in a wider temperature range of 140 to 600 °C, with a much lower reaction rate than that of cellulose [68].

In all the investigated cases, the reactions of the pseudo 2 contributed the main mass loss for the peak of the total reactions. On the other hand, the reactions of pseudo 1 happened in wider temperature ranges. These results have flatter peaks compared to the other results. Furthermore, the temperature ranges of pseudo 1 and pseudo 2 of AWD were all very close to that of the lignin and cellulose, separately. Thus, the deduced reactions of pseudo 1 and pseudo 2 of AWD should be mainly contributed by the thermal decompositions of lignin and cellulose, respectively.

It is observed from Table 4 that the HTC treatment increases the T_m values of the pseudo reactions of 1 & 2 for 22–24 °C and 20–21 °C, respectively. These findings are due to a smaller content of the organics with lower thermal stability in the hydrochar compared to that of AWD. Specifically, the higher T_m values of the pseudo 2 reactions of the hydrochar than that of AWD were caused by the remaining crystalline structure of cellulose and the crystalline arrangements by the free hydroxyl groups in cellulose and during the HTC process [69]. The following works will be focused on the pseudo 2 reactions because of their more significant reactions.

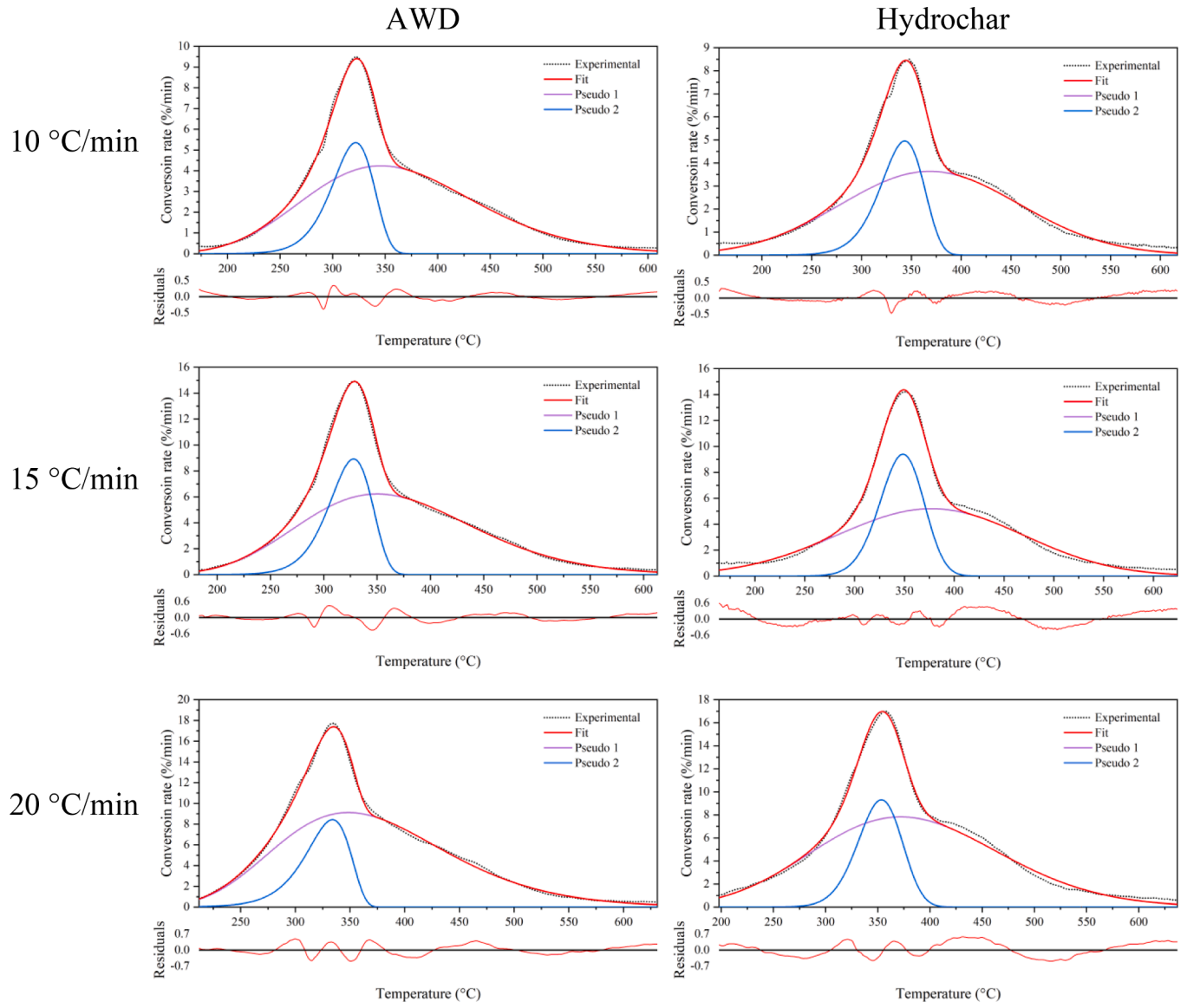

Fig. 7. Curves of conversion rates: experimental, pseudos, and the fitting, as well as the fitting residuals of the pyrolysis of AWD and its hydrochar under different heating rates.

Table 4
Parameters of the curves of the pseudo conversion rate deduced by using the Frazer-Suzuki deconvolution method.

		Pseudo 1			Pseudo 2		
Heating rate (°C/min)		10	15	20	10	15	20
AWD	h (%/min)	4.24	6.22	9.11	5.36	8.92	8.43
	a_s	0.18	0.18	0.25	−0.29	−0.29	−0.42
	T_m (°C)	346	350	348	322	328	334
	w_{hf} (°C)	189.79	190.09	180.98	46.82	47.27	47.09
Hydrochar	h (%/min)	3.63	5.20	7.83	4.95	9.40	9.31
	a_s	0.01	−0.03	0.10	−0.25	−0.10	−0.13
	T_m (°C)	368	377	372	343	349	354
	w_{hf} (°C)	211.31	220.89	211.06	50.72	52.01	49.94

3.4.2. *Kinetic plotting results of the pseudoreactions*

The deduced pseudo 2 reactions were selected for further kinetic and thermodynamic studies. The kinetic plotting results by using the Friedman, KAS, and OFW methods are given in Fig. 8. In the conversion rate range of 20% to 90%, the plotting of the pseudo 2 showed smoother results compared to that of the corresponding total reactions shown in Fig. 5. This is especially true when using the Friedman method. This is caused by two reasons:

1. The total reactions are more complex than their pseudoreactions as they represent the sum of their pseudoreactions.
2. By applying the mathematic deconvolution, some fluctuations will be neglected (which can be observed as the “residuals” as given in Fig. 7). Therefore, the curves of the deduced pseudoreactions are

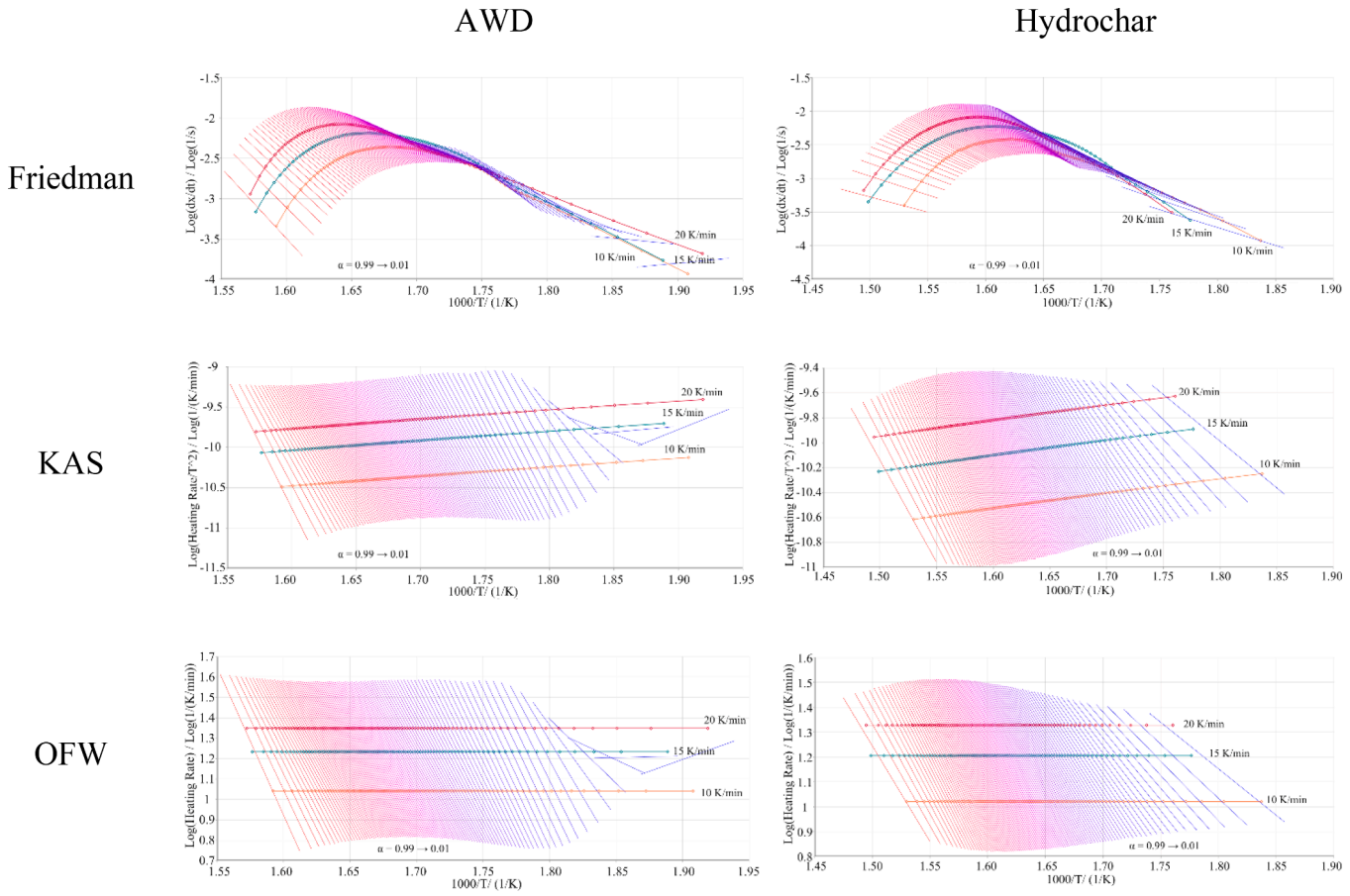

Fig. 8. Kinetic analysis of the pseudo 2 of the pyrolysis of AWD and hydrochar using the Friedman, KAS, and OFW methods.

smooth and can be seen as "perfect". Although this process will introduce errors, acceptable results with good fitting levels can be used to some extent.

The plotting results also indicate a successful deconvolution of the total reactions. Further kinetic and thermodynamic analysis based on these plotting results can provide a better understanding of the effect of the HTC treatment on the pyrolysis of AWD.

3.4.3. *Activation energies of the pseudoreactions*

The deduced activation energies and pre-exponential factors from the pseudo 2 by using the Friedman, KAS, and OFW methods are given in Fig. 9 and **Fig. S3**, respectively. The estimated mean values of the activation energies by using the three methods between the conversion rate of 20% to 90% are given in Table 5: The mean activation energy of the pseudo 2 reaction of AWD is decreased from 203.75 to 175.64 kJ/mol after the HTC treatment. Moreover, The process parameters and the kinetic results yielded by a series of related previous works are also listed in Table 5.

It can be seen that similar phenomena were also observed by Olszewski et al. [36], Ma et al. [70], Zhang et al. [71], and Li et al. [72]: they found that the HTC treatment of brewer's spent grains, sewage sludge, and waste lettuce would decrease the needed activation energies for the pyrolysis processes. Interestingly, opposite results were reported by the pyrolysis kinetic studies of sawdust [37 70 73], rice straw [71], and Karanj fruit hulls [74].

It was reported by Zhuang et al. that the typical hydrolyzing temperatures of hemicellulose, cellulose, and lignin have values in the range of 180 °C, 220–240 °C, and 210–300 °C, respectively [75]. Moreover, they also calculated the pyrolytic activation energies of pseudo hemicellulose, cellulose, and lignin of the herbal tea waste and its hydrochars produced at 120–300 °C: it was found that the HTC treatment could decrease the activation energies required for the pyrolysis of hemicellulose and cellulose while increasing that of lignin [75]. It has been known that compared to hemicellulose and cellulose, the highly branched aromatic structures of lignin impedes most of the biomass-to-bioenergy conversion processes [76]. Thus, the hydrolyzing reaction of lignin requires the highest temperature [77]. Therefore, the HTC treatment of lignocellulose-riched materials might not be positive for the following pyrolysis process, as it could increase the activation energy.

However, unlike the other lignocellulosic materials investigated previously as listed in Table 5, the pyrolytic activation energy of AWD was decreased after the HTC treatment. During the anaerobic digestion process, the lignin will first be depolymerized and solubilized to monomers and monoaromatic compounds [78]. Thereafter, these products will be cracked to smaller chemicals during further digestion [78]. As a result, the anaerobic digestion of lignocellulose materials should be beneficial for the pyrolysis of the corresponding hydrochar in the kinetic aspect, which stresses the importance of the research of pyrolysis of HTC-treated digestate.

3.4.4. *Thermodynamic results of the pseudoreactions*

To further investigate the influence of an HTC treatment on the pyrolysis of AWD, a thermodynamic analysis of the deduced pseudo 2 reactions was conducted. The mean values of the activation energies at different conversion rates calculated by using the Friedman, KAS, and OFW methods were adopted for the thermodynamic analysis. As shown by **Eq (10–12)**, the temperatures of each conversion rate and the peak temperature are needed for the thermodynamic calculations. However, these parameters are not consistent when different heating rates were applied (as shown in Table3). It is recommended that corresponding parameters yielded from the lowest heating rate should be used for the

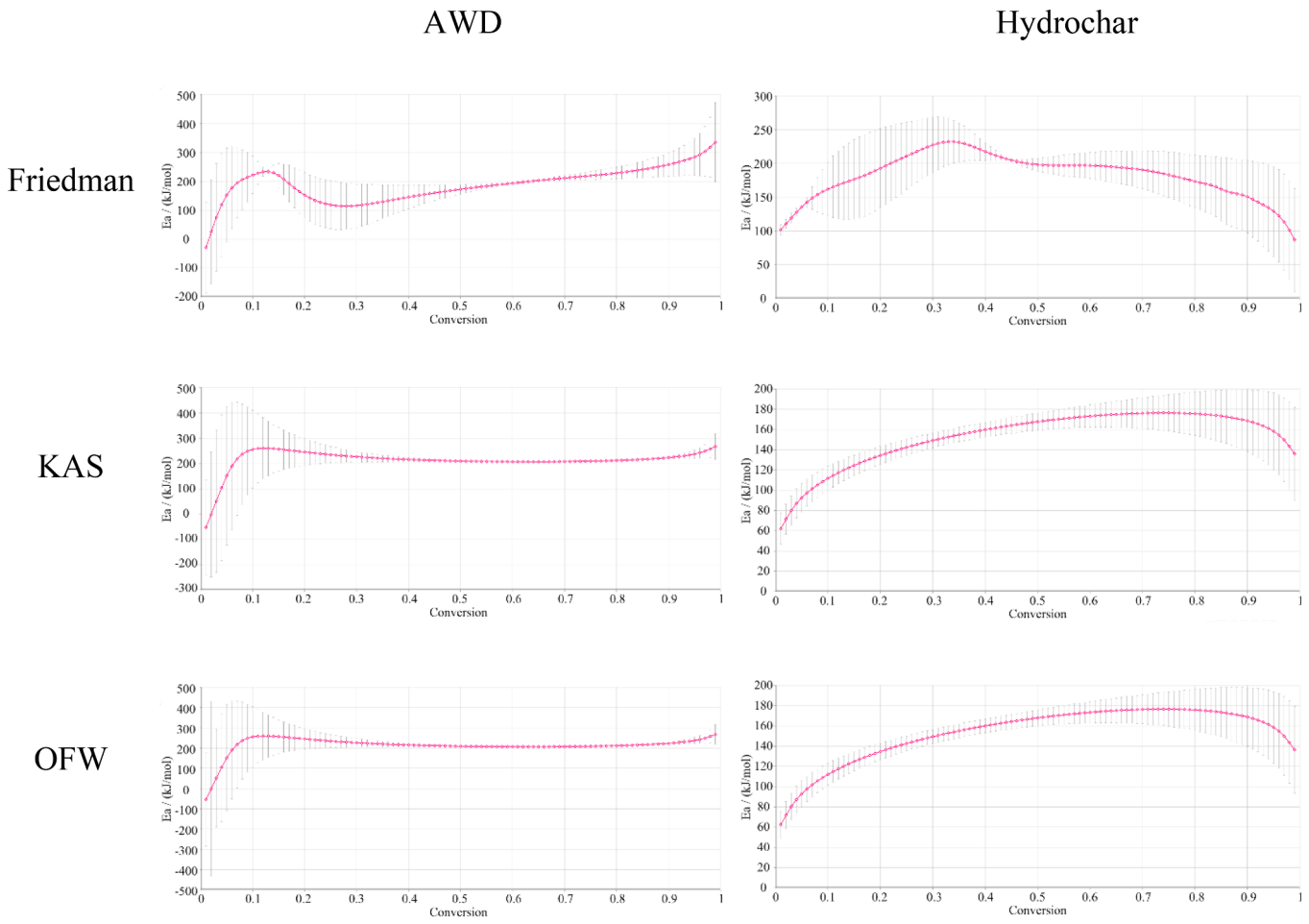

Fig. 9. Activation energy of the pseudo 2 of the pyrolysis of AWD and hydrochar deducing by using the Friedman, KAS, and OFW methods.

Table 5
The estimated activation energies of the pyrolysis of the raw and the HTC-treated feedstocks from current work and previous works.

	Raw materials	HTC		Pyrolysis		Kinetic analysis	
		Temperature (°C)	Time (h)	Temperature range (°C)	Heating rate (°C/min)	Methods	Activation energy (kJ/mol)
Current work	AWD (pseudo 2)	–	–	220–362	10	3 methods	
	AWD (pseudo 2)	–	–	225–366	15	3 methods	203.75
	AWD (pseudo 2)	–	–	229–370	20	3 methods	
	AWD (pseudo 2)	190	0.5	250–386	10	3 methods	
	AWD (pseudo 2)	190	0.5	258–403	15	3 methods	175.64
	AWD (pseudo 2)	190	0.5	264–408	20	3 methods	
Olszewski et al. [36]	Brewer's spent grains	–	–	105–800	5, 10, 20, 40	KAS	285
	Brewer's spent grains	180	4	105–800	5, 10, 20, 40	KAS	147
	Brewer's spent grains	220	2	105–800	5, 10, 20, 40	KAS	170
	Brewer's spent grains	220	4	105–800	5, 10, 20, 40	KAS	188
Li et al. [37]	Pinewood sawdust	–	–	290–420	30	Fn	58.64
	Pinewood sawdust	220	1	270–390	30	Fn	59.44
	Pinewood sawdust	240	1	340–420	30	Fn	63.33
	Pinewood sawdust	260	1	360–500	30	Fn	65.48
Ma et al. [70]	Sawdust	–	–	232.7–519.5	10, 20, 30, 40	OFW, KAS	173.32
	Sawdust	220	1	264.1–808.8	10, 20, 30, 40	OFW, KAS	184.63
	Sewage sludge	–	–	148.2–808.8	10, 20, 30, 40	OFW, KAS	311.87
	Sewage sludge	220	1	185.8–847.0	10, 20, 30, 40	OFW, KAS	221.07
Zhang et al. [71]	Rice straw	–	–	219.1–431.3	10, 20, 30, 40	KAS	222.73
	Rice straw	200	2	251.5–505.2	10, 20, 30, 40	KAS	233.27
	Sewage sludge	–	–	157.3–614.2	10, 20, 30, 40	KAS	477.10
	Sewage sludge	200	2	165.3–638.5	10, 20, 30, 40	KAS	394.02
Kabakcı et al. [73]	Sawdust	–	–	~180 - ~580	10, 20, 30, 40	Friedman	151.94
	Sawdust	220	1.5	~170 - ~570	10, 20, 30, 40	Friedman	157.17
Islam et al. [74]	Karanj fruit hulls	–	–	30–850	5, 10, 20	OFW, KAS	64.80
	Karanj fruit hulls	200	5	30–850	5, 10, 20	OFW, KAS	133.18
Li et al. [72]	Waste lettuce	–	–	173–588	20	Fn	68.3
	Waste lettuce	240	2	140–700	20	Fn	38.5

thermodynamic calculations as they were more accurate than that of higher heating rates [79]. Therefore, the related parameters obtained from the results of 10 °C/min were applied for the thermodynamic estimations. The deduced $\Delta H^{\ddagger}$, $\Delta S^{\ddagger}$, and $\Delta G^{\ddagger}$ values of the pyrolysis of the pseudo 2 of AWD and its hydrochar during conversion rates between 0.2 and 0.8 are shown in Fig. 10.

The $\Delta H^{\ddagger}$ represents the total heat transferring during the reactions [80]. The HTC treatment decreased the mean $\Delta H^{\ddagger}$ values of the pseudo 2 of the pyrolysis of AWD from 197.97 kJ/mol to 169.68 kJ/mol. This agreed with the decrease of the activation energies as shown in Fig. 9 and Table 4. Furthermore, the results illustrated that the HTC treatment could reduce the heat needed for the reactants of the pseudo 2 reactions of the AWD pyrolysis to reach their activating status. Thus, the HTC treatment can favor the pyrolysis of AWD with respect to $\Delta H^{\ddagger}$.

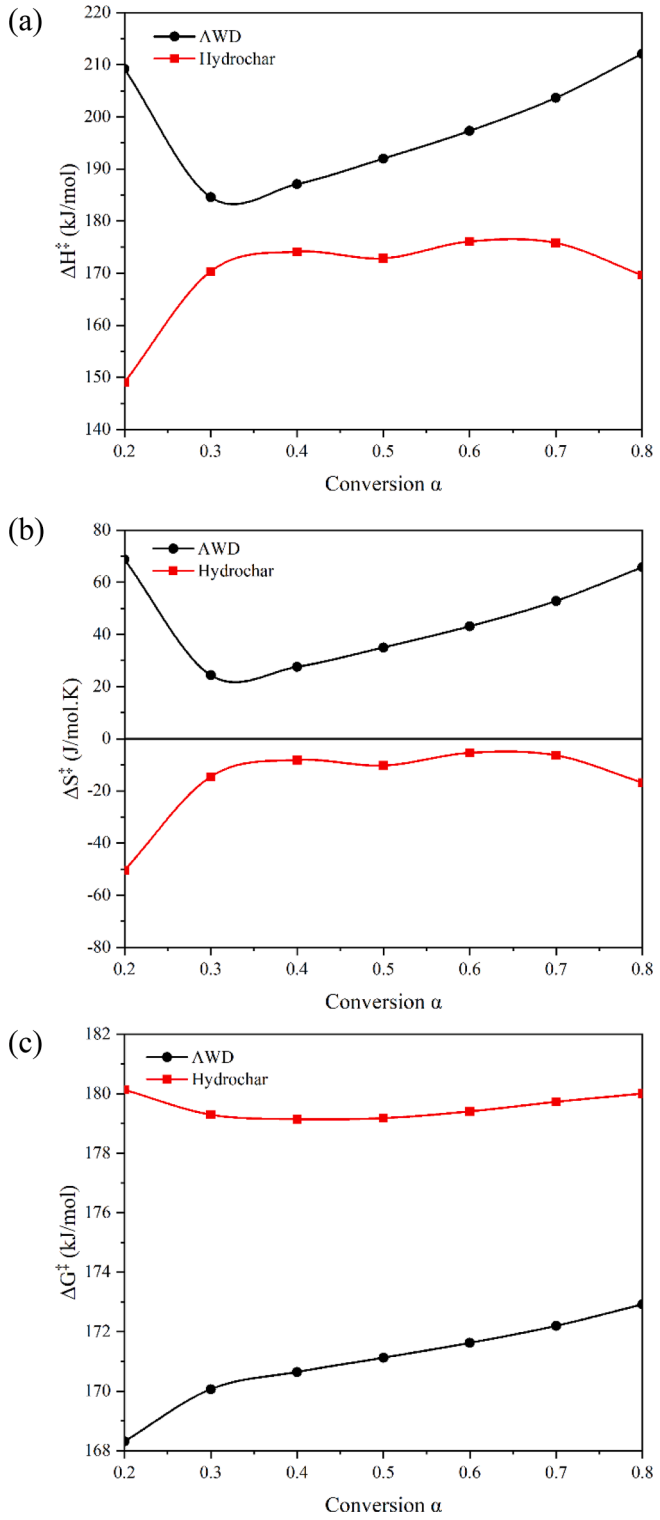

Fig. 10. (a) $\Delta H\ddagger$, (b) $\Delta S\ddagger$, and (c) $\Delta G\ddagger$ of the pyrolysis of the pseudo 2 of AWD and its hydrochar.

On the contrary, when considering the aspect of $\Delta S^{\ddagger}$, the pseudo 2 reaction of the pyrolysis of hydrochar was harder to reach its activating status than AWD. The $\Delta S^{\ddagger}$ value can be used to evaluate how close the thermodynamic equilibrium of a process is [81]. A higher value of $\Delta S^{\ddagger}$ corresponds to a higher disorder degree and thus, favors the reactions [82]. From the $\Delta S^{\ddagger}$ results in Fig. 10, it can be seen that the values of $\Delta S^{\ddagger}$ of the pseudo 2 reaction of pyrolysis of AWD are positive while that of hydrochar are negative. A similar result was also observed by Ma et al., who found that the mean values of $\Delta S^{\ddagger}$ of the pyrolysis of sewage sludge decreased from 270.00 J/mol.K to 52.62 J/mol.K [70].

$\Delta G^{\ddagger}$ represents the increment of the total system energy to form the activated complex [83]. From the definition of $\Delta G^{\ddagger}$ by **Eq. (11)**, it can be seen as a parameter that integrates the aspects of $\Delta H^{\ddagger}$ and $\Delta S^{\ddagger}$ to evaluate the natural direction of a reaction. As shown in Fig. 10, the pseudo 2 reaction of the pyrolysis of hydrochar had higher $\Delta G^{\ddagger}$ values to form the activated complex compared to that of AWD during the conversion rates investigated. These can be reflected in the higher temperature ranges (Table 5) and the higher peak temperatures (Table 4) of the reactions.

3.5. Kinetic predictions

The produced kinetic parameters can be used for interpolation and extrapolation [84]: the most important practical application of the kinetic analysis is the kinetic predictions [46] as the produced results can be used for process optimizations [85]. Furthermore, kinetic predictions could also help to analyze the complexity of the composition [49]. In this study, the obtained kinetic parameters of the total pyrolysis reactions of AWD and its hydrochar were used to predict their isothermal performances. The results can be an essential reference for further studies and applications of the pyrolysis of AWD and its hydrochar, especially when investigating the HTC treatment's effect on the whole process design and simulations. This would also be our next research topic.

3.5.1. Model selection

Three model-free methods were used in this study. The usage of sound kinetic models is critical for the reliability of the deduced kinetic predictions and it is recommended by ICTAC to reconstruct the kinetic results and compare them with available experimental data [46]. Hence, the fitting results are needed for the selection and the verification of the method to enable further kinetic predictions. By using **Eq. (5)**, the simulated conversion curves can be reconstructed based on the yielded kinetic results. Fig. 11 gives the fitting results of the conversion curves of the total pyrolytic reactions of AWD and its hydrochar when using the three methods. All the cases showed an acceptable result with R^2 values higher than 0.98. However, the fitting results of the pyrolysis of AWD and its hydrochar by using the Friedman method deduced the highest R^2 values that both equated to 0.9999. This was because the Friedman method could yield kinetic parameters with a better accuracy compared to when the KAS and OFW methods were used [86]. Therefore, the results produced by using the Friedman method were applied for the kinetic predictions. These highly fitting results also confirmed the reliability of the kinetic and thermodynamic studies in this study. Moreover, the corresponding thermodynamic parameters including the $\Delta H^{\ddagger}$, $\Delta S^{\ddagger}$, and $\Delta G^{\ddagger}$ values of the total pyrolysis reactions of AWD and its hydrochar were also calculated based on Friedman's results. These data are also given in **Fig. S4** as a reference.

3.5.2. Kinetic isothermal predictions

According to the isothermal prediction results shown in Fig. 12, the

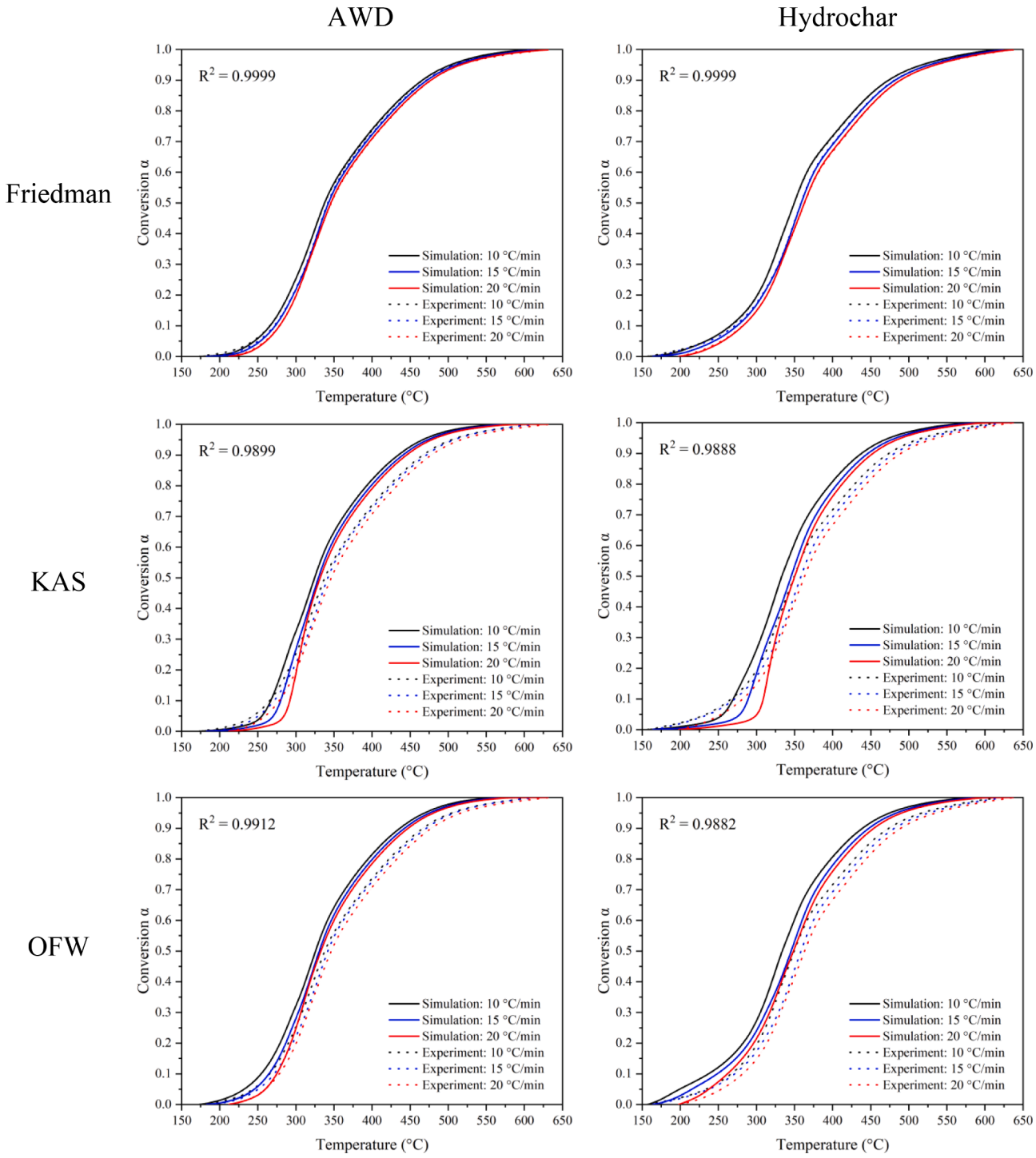

Fig. 11. Experimental and simulating conversion curves of AWD and its hydrochar deducing by using the Friedman, KAS, and OFW methods.

reactions can be considered to commence when the temperature is higher than 350 °C [87]. Interestingly, the results for a temperature of 350 °C were also close to all the peak temperatures of the deduced pseudo 2 reactions as shown in Table 3. Thus, these results indicate the reliability of the deconvolution, kinetic, and thermodynamic results of the pseudoreactions to some extent. Based on the isothermal prediction plotting cases investigated in this study, the temperature of 450 °C was recommended to be applied as the minimum peak temperature for the bench-scale research and for further applications. This is due to the that when the temperature was 450 °C, the conversion rates of the pyrolytic reactions of AWD and its hydrochar will exceed 90% in only 4.21 and 5.94 min, respectively. Moreover, when the isothermal time was 30 min, the conversion rates of the AWD and its hydrochar pyrolysis reached values of 94.92% and 94.60%, separately. Thus, the reaction levels of the pyrolysis of AWD and its hydrochar at 450 °C were acceptable when the isothermal time exceeded 6 min. On the other hand, when the isothermal temperature was 400 °C, the conversion rates of the two reactions were still lower than 90% even after 30 min.

The results of the corresponding kinetic dynamic predictions of the pyrolysis of ADW and its hydrochar are also given in **Fig. S5** as a reference. The dynamic performances of the two pyrolysis reactions under 6 different heating rates of 1, 2, 4, 8, 16, and 32 °C/min were

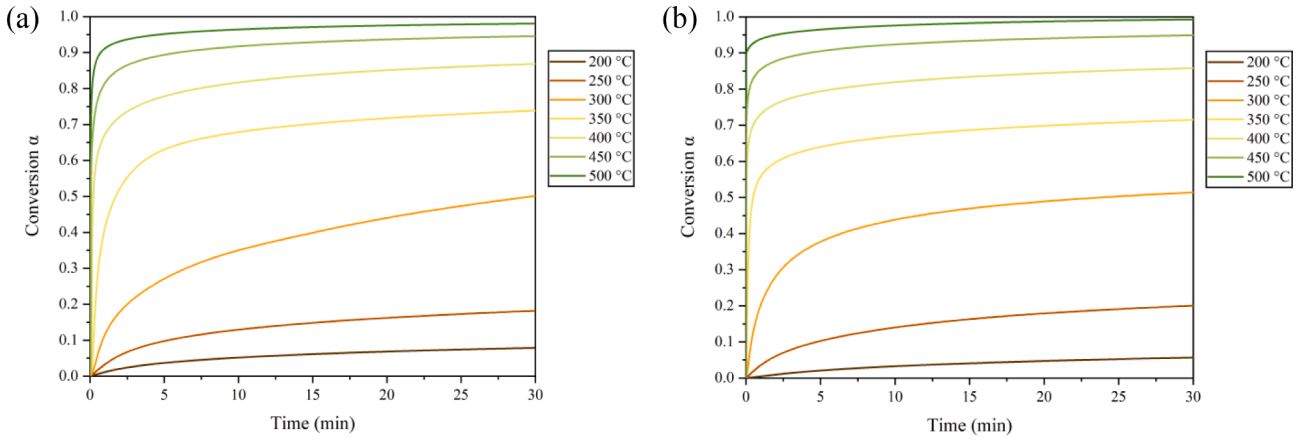

Fig. 12. Predicted curves of isothermal conversion of pyrolysis of (a) AWD and (b) hydrochar at 200, 250, 300, 350, 400, 450, and 500 °C based on the kinetic parameters estimated by using the Friedman method.

predicted.

4. Conclusion

In this work, the impacts of HTC treatments on the kinetics and thermodynamics of the pyrolysis of AWD and its hydrochar were evaluated. The main discoveries can be summarized as follows:

- An HTC treatment decreased the ratios of O/C and H/C of AWD from 0.36 and 1.31 to 0.35 and 1.22, respectively.
- An HTC treatment can decrease the pyrolytic activation energies of AWD: from the ranges of 182.91–274.43 kJ/mol to 144.59–205.20 kJ/mol by using the Friedman method.
- Specifically, for the pseudo 2 reactions deduced in this study, the mean activation energy decreased from 203.75 to 175.64 kJ/mol after the HTC treatment.
- The process of anaerobic digestion of lignocellulose materials might be beneficial for the pyrolysis of hydrochar as it could decrease the pyrolytic activation energy.
- The hydrochar required about 28.29 kJ/mol less of an average $\Delta H^{\ddagger}$ value compared to when using AWD to form the activated complex for the pseudo 2 pyrolysis reaction. This corresponds to the lower activation energy of the pyrolysis of hydrochar compared to that of AWD.
- The kinetic prediction results can be used to optimize the process development. A value of 450 °C was suggested to be the minimum peak temperature for the further related larger-scale and/or process simulation investigations.

Based on the kinetic and thermodynamic results, future studies of the impact of an HTC treatment on the pyrolysis of AWD would be conducted by bench-scale experiments and process simulations.

Declaration of Competing Interest

The authors declare that they have no known competing financial interests or personal relationships that could have appeared to influence the work reported in this paper.

Acknowledgments

The authors would like to thank the European Commission, the National Centre for Research and Development (Poland), Nederlandse Organisatie Voor Wetenschappelijk Onderzoek (Netherlands), and Swedish Research Council Formas for funding in the frame of the collaborative international consortium (RECOWATDIG) financed under the 2018 Joint call of the WaterWorks2017 ERA-NET Cofund. This ERA-NET is an integral part of the activities developed by the Water JPI. National Centre for Research and Development agreement number WATERWORKS2017/I/RECOWATDIG/01/2019. The first author, Shule Wang, would like to acknowledge the financial support from the Chinese Scholarship Council (CSC) for the support of this study. The corresponding author, Yuming Wen, would like to thank Chuchu Tang and Yan Li for helping with the drawing of Graphical Abstract and Fig. 1, respectively.

Appendix A. Supplementary data

Supplementary data to this article can be found online at https://doi.org/10.1016/j.cej.2021.133881.

References

[1] J.G. Speight, 5 - Sources of water pollution, in: J.G. Speight (Ed.) Natural Water Remediation, Butterworth-Heinemann2020, pp. 165–198.
[2] F.G. Fermoso, A. Serrano, B. Alonso-Fariñas, J. Fernández-Bolaños, R. Borja, G. Rodríguez-Gutiérrez, Valuable Compound Extraction, Anaerobic Digestion, and Composting: A Leading Biorefinery Approach for Agricultural Wastes, J. Agric. Food. Chem. 66 (2018) 8451–8468.
[3] S. Achinas, G.J.W. Euverink, Theoretical analysis of biogas potential prediction from agricultural waste, Resour.-Effic. Technol. 2 (3) (2016) 143–147.
[4] S.M. El-Haggar, Chapter 7 - Sustainability of Agricultural and Rural Waste Management, in: S.M. El-Haggar (Ed.), Sustainable Industrial Design and Waste Management, Academic Press, Oxford, 2007, pp. 223–260.
[5] A. Crolla, C. Kinsley, E. Pattey, Land application of digestate, Elsevier, The biogas handbook, 2013, pp. 302–325.
[6] D. Huygens, G. Orveillon, E. Lugato, S. Tavazzi, S. Comero, A. Jones, B. Gawlik, H. Saveyn, Technical proposals for the safe use of processed manure above the threshold established for Nitrate Vulnerable Zones by the Nitrates Directive (91/676/EEC), JRC121636.[Google Scholar] (2020) 170.
[7] Y. Wen, Z. Shi, S. Wang, W. Mu, P.G. Jönsson, W. Yang, Pyrolysis of raw and anaerobically digested organic fractions of municipal solid waste: Kinetics, thermodynamics, and product characterization, Chem. Eng. J. 415 (2021), 129064.
[8] J. Liu, S. Huang, K. Chen, T. Wang, M. Mei, J. Li, Preparation of biochar from food waste digestate: Pyrolysis behavior and product properties, Bioresour. Technol. 302 (2020), 122841.
[9] J. González-Arias, M.V. Gil, R.Á. Fernández, E.J. Martínez, C. Fernández, G. Papaharalabos, X. Gómez, Integrating anaerobic digestion and pyrolysis for treating digestates derived from sewage sludge and fat wastes, Environ. Sci. Pollut. Res. Int. 27 (26) (2020) 32603–32614.
[10] E. Miliotti, D. Casini, L. Rosi, G. Lotti, A.M. Rizzo, D. Chiaramonti, Lab-scale pyrolysis and hydrothermal carbonization of biomass digestate: Characterization of solid products and compliance with biochar standards, Biomass Bioenergy 139 (2020), 105593.
[11] S. Tayibi, F. Monlau, F. Marias, G. Cazaudehore, N.-E. Fayoud, A. Oukarroum, Y. Zeroual, A. Barakat, Coupling anaerobic digestion and pyrolysis processes for maximizing energy recovery and soil preservation according to the circular economy concept, J. Environ. Manage. 279 (2021), 111632.
[12] S. Tayibi, F. Monlau, F. Marias, N. Thevenin, R. Jimenez, A. Oukarroum, A. Alboulkas, Y. Zeroual, A. Barakat, Industrial symbiosis of anaerobic digestion and pyrolysis: Performances and agricultural interest of coupling biochar and

liquid digestate, Sci. Total Environ. 793 (2021) 148461, https://doi.org/10.1016/j.scitotenv.2021.148461.
[13] V. Chaturvedi, S. Usangonvkar, M.V. Shelke, Synthesis of high surface area porous carbon from anaerobic digestate and it's electrochemical study as an electrode material for ultracapacitors, RSC Adv. 9 (62) (2019) 36343–36350.
[14] F. Monlau, M. Francavilla, C. Sambusiti, N. Antoniou, A. Solhy, A. Libutti, A. Zabaniotou, A. Barakat, M. Monteleone, Toward a functional integration of anaerobic digestion and pyrolysis for a sustainable resource management. Comparison between solid-digestate and its derived pyrochar as soil amendment, Appl. Energy 169 (2016) 652–662.
[15] E. Gul, K. Al Bkoor Alrawashdeh, O. Masek, Ø. Skreiberg, A. Corona, M. Zampilli, L. Wang, P. Samaras, Q. Yang, H. Zhou, P. Bartocci, F. Fantozzi, Production and use of biochar from lignin and lignin-rich residues (such as digestate and olive stones) for wastewater treatment, J. Anal. Appl. Pyrol. 158 (2021) 105263, https://doi.org/10.1016/j.jaap.2021.105263.
[16] S.A. Opatokun, V. Strezov, T. Kan, Product based evaluation of pyrolysis of food waste and its digestate, Energy 92 (2015) 349–354.
[17] E. Leijenhorst, Pyrolysis of Agro-Digestate: Nutrient Distribution, in: E. Meers, G. Velthof, E. Michels, R. Rietra (Eds.), Biorefinery of Inorganics: Recovering Mineral Nutrients from Biomass and Organic Waste, Wiley, 2020, pp. 133–146, https://doi.org/10.1002/9781118921487.ch4-3.
[18] V.S. Sikarwar, M. Pohořelý, E. Meers, S. Skoblia, J. Moško, M. Jeremiáš, Potential of coupling anaerobic digestion with thermochemical technologies for waste valorization, Fuel 294 (2021), 120533.
[19] C. Maurer, J. Müller, Drying characteristics of biogas digestate in a hybrid waste-heat/solar dryer, Energies 12 (2019) 1294.
[20] Y. Shen, A review on hydrothermal carbonization of biomass and plastic wastes to energy products, Biomass Bioenergy 134 (2020), 105479.
[21] C. Aragón-Briceño, A.B. Ross, M.A. Camargo-Valero, Evaluation and comparison of product yields and bio-methane potential in sewage digestate following hydrothermal treatment, Appl. Energy 208 (2017) 1357–1369.
[22] M. Wilk, A. Magdziarz, K. Jayaraman, M. Szymańska-Chargot, I. Gökalp, Hydrothermal carbonization characteristics of sewage sludge and lignocellulosic biomass. A comparative study, Biomass Bioenergy 120 (2019) 166–175.
[23] M. Śliz, M. Wilk, A comprehensive investigation of hydrothermal carbonization: Energy potential of hydrochar derived from Virginia mallow, Renewable Energy 156 (2020) 942–950.
[24] C. He, C. Tang, C. Li, J. Yuan, K.-Q. Tran, Q.-V. Bach, R. Qiu, Y. Yang, Wet torrefaction of biomass for high quality solid fuel production: A review, Renew. Sustain. Energy Rev. 91 (2018) 259–271.
[25] S. Wang, H. Persson, W. Yang, P.G. Jönsson, Pyrolysis study of hydrothermal carbonization-treated digested sewage sludge using a Py-GC/MS and a bench-scale pyrolyzer, Fuel 262 (2020), 116335.
[26] D. Zhang, F. Wang, X. Shen, W. Yi, Z. Li, Y. Li, C. Tian, Comparison study on fuel properties of hydrochars produced from corn stalk and corn stalk digestate, Energy 165 (2018) 527–536.
[27] M. Bernardo, C.R. Correa, Y. Ringelspacher, G.C. Becker, N. Lapa, I. Fonseca, I.A.A. C. Esteves, A. Kruse, Porous carbons derived from hydrothermally treated biogas digestate, Waste Manage. 105 (2020) 170–179.
[28] K.R. Parmar, A.B. Ross, Integration of hydrothermal carbonisation with anaerobic digestion; Opportunities for valorisation of digestate, Energies 12 (2019) 1586.
[29] Z. Cao, B. Hülsemann, D. Wüst, L. Illi, H. Oechsner, A. Kruse, Valorization of maize silage digestate from two-stage anaerobic digestion by hydrothermal carbonization, Energy Convers. Manage. 222 (2020), 113218.
[30] H.S. Kambo, A. Dutta, Strength, storage, and combustion characteristics of densified lignocellulosic biomass produced via torrefaction and hydrothermal carbonization, Appl. Energy 135 (2014) 182–191.
[31] H. Pawlak-Kruczek, A. Urbanowska, W. Yang, G. Brem, A. Magdziarz, P. Seruga, L. Niedzwiecki, A. Pozarlik, A. Mlonka-Mędrala, M. Kabsch-Korbutowicz, Industrial process description for the Recovery of agricultural water from digestate, J. Energy Res. Technol. 142 (2020), 070917.
[32] A. Urbanowska, M. Kabsch-Korbutowicz, M. Wnukowski, P. Seruga, M. Baranowski, H. Pawlak-Kruczek, M. Serafin-Tkaczuk, K. Krochmalny, L. Niedzwiecki, Treatment of liquid by-products of hydrothermal carbonization (HTC) of agricultural digestate using membrane separation, Energies 13 (2020) 262.
[33] J. Stemann, F. Ziegler, Assessment of the energetic efficiency of a continuously operating plant for hydrothermal carbonisation of biomass, World Renewable Energy Congress-Sweden; 8–13 May; 2011, Linköping University Electronic Press, Linköping; Sweden, 2011, pp. 125–132.
[34] R.K. Garlapalli, B. Wirth, M.T. Reza, Pyrolysis of hydrochar from digestate: Effect of hydrothermal carbonization and pyrolysis temperatures on pyrochar formation, Bioresour. Technol. 220 (2016) 168–174.
[35] M.P. Olszewski, S.A. Nicolae, P.J. Arauzo, M.-M. Titirici, A. Kruse, Wet and dry? Influence of hydrothermal carbonization on the pyrolysis of spent grains, J. Cleaner Prod. 260 (2020), 121101.
[36] M.P. Olszewski, P.J. Arauzo, P.A. Maziarka, F. Ronsse, A. Kruse, Pyrolysis kinetics of hydrochars produced from Brewer's spent grains, Catalysts 9 (2019) 625.
[37] J. Li, P. Zhao, T. Li, M. Lei, W. Yan, S. Ge, Pyrolysis behavior of hydrochar from hydrothermal carbonization of pinewood sawdust, J. Anal. Appl. Pyrol. 146 (2020), 104771.
[38] A. Soria-Verdugo, M.T. Morgano, H. Mätzing, E. Goos, H. Leibold, D. Merz, U. Riedel, D. Stapf, Comparison of wood pyrolysis kinetic data derived from thermogravimetric experiments by model-fitting and model-free methods, Energy Convers. Manage. 212 (2020), 112818.
[39] S.R. Naqvi, R. Tariq, Z. Hameed, I. Ali, S.A. Taqvi, M. Naqvi, M. Niazi, T. Noor, W. Farooq, Pyrolysis of high-ash sewage sludge: Thermo-kinetic study using TGA and artificial neural networks, Fuel 233 (2018) 529–538.
[40] A.K. Varma, N. Lal, A.K. Rathore, R. Katiyar, L.S. Thakur, R. Shankar, P. Mondal, Thermal, kinetic and thermodynamic study for co-pyrolysis of pine needles and styrofoam using thermogravimetric analysis, Energy 218 (2021), 119404.
[41] H. Stančin, H. Mikulčić, N. Manić, D. Stojiljiković, M. Vujanović, X. Wang, N. Duić, Thermogravimetric and kinetic analysis of biomass and polyurethane foam mixtures Co-Pyrolysis, Energy 237 (2021), 121592.
[42] Z. Cao, D. Jung, M.P. Olszewski, P.J. Arauzo, A. Kruse, Hydrothermal carbonization of biogas digestate: Effect of digestate origin and process conditions, Waste Manag 100 (2019) 138–150.
[43] J.D.S. Castro, E.G.P. da Silva, C.F. Virgens, Evaluation of models to predict the influence of chemical pretreatment on the peels of Nephelium lappaceum L. based on pyrolysis kinetic parameters obtained using a combined Fraser-Suzuki function and Friedman's isoconversional method, J. Anal. Appl. Pyrol. 149 (2020), 104827.
[44] H. Liu, G. Xu, G. Li, Pyrolysis characteristic and kinetic analysis of sewage sludge using model-free and master plots methods, Process Saf. Environ. Prot. 149 (2021) 48–55.
[45] M.S. Ahmad, J.J. Klemeš, H. Alhumade, A. Elkamel, A. Mahmood, B. Shen, M. Ibrahim, A. Mukhtar, S. Saqib, S. Asif, Thermo-kinetic study to elucidate the bioenergy potential of Maple Leaf Waste (MLW) by pyrolysis, TGA and kinetic modelling, Fuel 293 (2021), 120349.
[46] S. Vyazovkin, A.K. Burnham, J.M. Criado, L.A. Pérez-Maqueda, C. Popescu, N. Sbirrazzuoli, ICTAC Kinetics Committee recommendations for performing kinetic computations on thermal analysis data, Thermochim. Acta 520 (1-2) (2011) 1–19.
[47] H. Shahbeig, M. Nosrati, Pyrolysis of municipal sewage sludge for bioenergy production: thermo-kinetic studies, evolved gas analysis, and techno-socio-economic assessment, Renew. Sustain. Energy Rev. 119 (2020), 109567.
[48] C.-G. Chao, H.-L. Chiang, C.-Y. Chen, Pyrolytic kinetics of sludge from a petrochemical factory wastewater treatment plant—a transition state theory approach, Chemosphere 49 (4) (2002) 431–437.
[49] G. Mishra, J. Kumar, T. Bhaskar, Kinetic studies on the pyrolysis of pinewood, Bioresour. Technol. 182 (2015) 282–288.
[50] J.-H. Zhang, Q.-M. Lin, X.-R. Zhao, The Hydrochar Characters of Municipal Sewage Sludge Under Different Hydrothermal Temperatures and Durations, Journal of Integrative, Agriculture 13 (3) (2014) 471–482.
[51] M. Wu, P. Li, G. Li, E. Petropoulos, Y. Feng, Z. Li, The chemodiversity of paddy soil dissolved organic matter is shaped and homogenized by bacterial communities that are orchestrated by geographic distance and fertilizations, Soil Biol. Biochem. 161 (2021) 108374, https://doi.org/10.1016/j.soilbio.2021.108374.
[52] C. Nzediegwu, M. Arshad, A. Ulah, M.A. Naeth, S.X. Chang, Fuel, thermal and surface properties of microwave-pyrolyzed biochars depend on feedstock type and pyrolysis temperature, Bioresour. Technol. 320 (2021), 124282.
[53] A. Funke, F. Ziegler, Hydrothermal carbonization of biomass: a summary and discussion of chemical mechanisms for process engineering, Biofuels, Bioprod. Biorefin. 4 (2) (2010) 160–177.
[54] P. Zhang, S.-J. Dong, H.-H. Ma, B.-X. Zhang, Y.-F. Wang, X.-M. Hu, Fractionation of corn stover into cellulose, hemicellulose and lignin using a series of ionic liquids, Ind. Crops Prod. 76 (2015) 688–696.
[55] M. Volpe, A. Messineo, M. Mäkelä, M.R. Barr, R. Volpe, C. Corrado, L. Fiori, Reactivity of cellulose during hydrothermal carbonization of lignocellulosic biomass, Fuel Process. Technol. 206 (2020), 106456.
[56] J. He, V. Strezov, X. Zhou, R. Kumar, H. Weldekidan, T. Kan, Effects of co-pyrolysis of heavy metal contaminated biomass with magnesium carbonate on heavy metal deportment and pyrolytic product properties, Fuel 294 (2021), 120545.
[57] W. Tao, W. Duan, C. Liu, D. Zhu, X. Si, R. Zhu, P. Oleszczuk, B. Pan, Formation of persistent free radicals in biochar derived from rice straw based on a detailed analysis of pyrolysis kinetics, Sci. Total Environ. 715 (2020), 136575.
[58] T. Rasool, I. Najar, V.C. Srivastava, A. Pandey, Pyrolysis of almond (Prunus amygdalus) shells: Kinetic analysis, modelling, energy assessment and technical feasibility studies, Bioresour. Technol. 337 (2021), 125466.
[59] S. Hidayat, M.S.A. Bakar, A. Ahmed, D.A. Iryani, M. Hussain, F. Jamil, Y.-K. Park, Comprehensive kinetic study of Imperata Cylindrica pyrolysis via Asym2sig deconvolution and combined kinetics, J. Anal. Appl. Pyrol. 156 (2021), 105133.
[60] S. Yousef, J. Eimontas, N. Striūgas, M.A. Abdelnaby, Influence of carbon black filler on pyrolysis kinetic behaviour and TG-FTIR-GC–MS analysis of glass fibre reinforced polymer composites, Energy 233 (2021) 121167, https://doi.org/10.1016/j.energy.2021.121167.
[61] H. Fan, J. Gu, Y. Wang, H. Yuan, Y. Chen, B. Luo, Effect of potassium on the pyrolysis of biomass components: Pyrolysis behaviors, product distribution and kinetic characteristics, Waste Manage. 121 (2021) 255–264.
[62] S. Wang, H. Lin, B. Ru, G. Dai, X. Wang, G. Xiao, Z. Luo, Kinetic modeling of biomass components pyrolysis using a sequential and coupling method, Fuel 185 (2016) 763–771.
[63] B. Lin, J. Zhou, Q. Qin, C. Xie, Z. Luo, Isoconversional kinetic analysis of overlapped pyrolysis reactions: The case of lignocellulosic biomass and blends with anthracite, J. Energy Inst. 95 (2021) 143–153.
[64] A. Perejón, P.E. Sánchez-Jiménez, C. García-Garrido, L.A. Pérez-Maqueda, Kinetic study of complex processes composed of non-independent stages: pyrolysis of natural rubber, Polym. Degrad. Stab. 188 (2021) 109590, https://doi.org/10.1016/j.polymdegradstab.2021.109590.
[65] S. Varsha, A.K. Vuppaladadiyam, F. Shehzad, H. Ghaedi, S. Murugavelh, W. Dong, E. Antunes, Co-pyrolysis of microalgae and municipal solid waste: A

thermogravimetric study to discern synergy during co-pyrolysis process, J. Energy Inst. 94 (2021) 29–38.
[66] K.K. Gupta, K.R. Aneja, D. Rana, Current status of cow dung as a bioresource for sustainable development, Bioresources and Bioprocessing 3 (2016) 1–11.
[67] C. Sambusiti, F. Monlau, E. Ficara, A. Musatti, M. Rollini, A. Barakat, F. Malpei, Comparison of various post-treatments for recovering methane from agricultural digestate, Fuel Process. Technol. 137 (2015) 359–365.
[68] S.D. Stefanidis, K.G. Kalogiannis, E.F. Iliopoulou, C.M. Michailof, P.A. Pilavachi, A. A. Lappas, A study of lignocellulosic biomass pyrolysis via the pyrolysis of cellulose, hemicellulose and lignin, J. Anal. Appl. Pyrol. 105 (2014) 143–150.
[69] X. Zhuang, H. Zhan, Y. Song, C. He, Y. Huang, X. Yin, C. Wu, Insights into the evolution of chemical structures in lignocellulose and non-lignocellulose biowastes during hydrothermal carbonization (HTC), Fuel 236 (2019) 960–974.
[70] J. Ma, H. Luo, Y.i. Li, Z. Liu, D. Li, C. Gai, W. Jiao, Pyrolysis kinetics and thermodynamic parameters of the hydrochars derived from co-hydrothermal carbonization of sawdust and sewage sludge using thermogravimetric analysis, Bioresour. Technol. 282 (2019) 133–141.
[71] S. Zhang, M. Pi, Y. Su, D. Xu, Y. Xiong, H. Zhang, Physiochemical properties and pyrolysis behavior evaluations of hydrochar from co-hydrothermal treatment of rice straw and sewage sludge, Biomass Bioenergy 140 (2020), 105664.
[72] Y. Li, H. Liu, K. Xiao, M. Jin, H. Xiao, H. Yao, Combustion and pyrolysis characteristics of hydrochar prepared by hydrothermal carbonization of typical food waste: influence of carbohydrates, proteins, and lipids, Energy Fuels 34 (2019) 430–439.
[73] S.B. Kabakcı, Pyrolysis and combustion characteristics and kinetics of wood sawdust and wood sawdust hydrochar, Environ. Prog. Sustainable Energy 39 (2) (2020), https://doi.org/10.1002/ep.v39.210.1002/ep.13315.
[74] M.A. Islam, M. Asif, B.H. Hameed, Pyrolysis kinetics of raw and hydrothermally carbonized Karanj (Pongamia pinnata) fruit hulls via thermogravimetric analysis, Bioresour. Technol. 179 (2015) 227–233.
[75] X. Zhuang, Y. Song, H. Zhan, X.T. Bi, X. Yin, C. Wu, Pyrolytic conversion of biowaste-derived hydrochar: decomposition mechanism of specific components, Fuel 266 (2020), 117106.
[76] C. Sawatdeenarunat, K.C. Surendra, D. Takara, H. Oechsner, S.K. Khanal, Anaerobic digestion of lignocellulosic biomass: challenges and opportunities, Bioresour. Technol. 178 (2015) 178–186.
[77] S. Wang, G. Dai, H. Yang, Z. Luo, Lignocellulosic biomass pyrolysis mechanism: a state-of-the-art review, Prog. Energy Combust. Sci. 62 (2017) 33–86.
[78] D.G. Mulat, S.J. Horn, Biogas production from lignin via anaerobic digestion, Lignin Valorization: Emerging Approaches, Energy Environ., series (2018) 391–412.
[79] H. Cao, Y.a. Xin, D. Wang, Q. Yuan, Pyrolysis characteristics of cattle manures using a discrete distributed activation energy model, Bioresour. Technol. 172 (2014) 219–225.
[80] M.S. Ahmad, C.-G. Liu, M. Nawaz, A. Tawab, X. Shen, B. Shen, M.A. Mehmood, Elucidating the pyrolysis reaction mechanism of Calotropis procera and analysis of pyrolysis products to evaluate its potential for bioenergy and chemicals, Bioresour. Technol. 322 (2021), 124545.
[81] R.K. Singh, T. Patil, A. Verma, S.P. Tekade, A.N. Sawarkar, Insights into kinetics, reaction mechanism, and thermodynamic analysis of pyrolysis of rice straw from rice bowl of India, Bioresour. Technol. Rep. 13 (2021), 100639.
[82] N. Rathore, A. Pawar, N. Panwar, Kinetic analysis and thermal degradation study on wheat straw and its biochar from vacuum pyrolysis under non-isothermal condition, Biomass Convers. Biorefin. (2021) 1–13.
[83] S. Gupta, P. Mondal, Catalytic pyrolysis of pine needles with nickel doped gamma-alumina: Reaction kinetics, mechanism, thermodynamics and products analysis, J. Cleaner Prod. 286 (2021), 124930.
[84] S. Vyazovkin, A.K. Burnham, L. Favergeon, N. Koga, E. Moukhina, L.A. Pérez-Maqueda, N. Sbirrazzuoli, ICTAC Kinetics Committee recommendations for analysis of multi-step kinetics, Thermochim Acta 689 (2020) 178597, https://doi.org/10.1016/j.tca.2020.178597.
[85] N. Manić, B. Janković, V. Dodevski, Model-free and model-based kinetic analysis of Poplar fluff (Populus alba) pyrolysis process under dynamic conditions, J. Therm. Anal. Calorim. 143 (5) (2021) 3419–3438.
[86] R.K. Mishra, K. Mohanty, X. Wang, Pyrolysis kinetic behavior and Py-GC–MS analysis of waste dahlia flowers into renewable fuel and value-added chemicals, Fuel 260 (2020), 116338.
[87] C.I. Akor, A.I. Osman, C. Farrell, C.S. McCallum, W.J. Doran, K. Morgan, J. Harrison, P.J. Walsh, G.N. Sheldrake, Thermokinetic study of residual solid digestate from anaerobic digestion, Chem. Eng. J. 406 (2021), 127039.